Radiative Transfer in the Earth Atmosphere: Community Radiative Transfer Model

Dr. Fuzhong Weng
Sensor Physics Branch
Center for Satellite Applications and Research
National Environmental Satellites, Data and Information Service
National Oceanic and Atmospheric Administration

2009 Update

Acknowledgements to CRTM Working Group

CRTM URLs

- CRTM trac page
  https://svnemc.ncep.noaa.gov/trac/crtm
- CRTM repository (for checkouts, commits, etc)
  https://svnemc.ncep.noaa.gov/projects/crtm

- CRTM ftp site
  ftp://ftp.emc.ncep.noaa.gov/jcsda/CRTM

- CRTM Announcement mailing list:
  https://lstsrv.ncep.noaa.gov/mailman/listinfo/ncep.list.emc.jcsda_crtm
- CRTM CWG mailing list:
  https://lstsrv.ncep.noaa.gov/mailman/listinfo/ncep.list.emc.jcsda_cwg
- CRTM Developers mailing list:
  https://lstsrv.ncep.noaa.gov/mailman/listinfo/ncep.list.emc.jcsda_crtm.developers

Acknowledgements

CRTM Members:	Organization	Areas of Expertise
Fuzhong Weng	STAR	CRTM technical oversight/emissivity
Yong Han	STAR	CRTM interface with NESDIS
Paul van Delst	NCEP	CRTM interface with NCEP
Ben Ruston	NRL	CRTM interface with NRL
Zhiquan Liu	NCAR/AFWA	CRTM interface with AFWA
Emily Liu	GMAO	CRTM interface with GMAO
Don Birkenhauer	OAR	CRTM interface with OAR
Ping Yang	Texas A&M	Cloud/aerosol scattering LUT
Ralf Bennarts	Univ Wisconsin	Transfer scheme
Jean-Luc Moncet	AER	Absorption model
Quanhua (Mark) Liu	Perot System	Transfer scheme
Banghua Yan	Perot System	Surface emissivity
Yong Chen	CIRA	validation/absorption model
David Groff	NCEP	transmittance data base
Ron Vogel	IMSG	IR surface emissivity
Jun Li	CIMSS	ABI retrieval algorithm
Tim Schmit	STAR	CRTM assessment
Tom Greenwalt	CIMSS	SOI

Outline

1. Radiative transfer model components
2. Radiative transfer schemes
3. Fast optical models for gas, aerosols, and clouds
4. Fast Zeeman effect model
5. Surface emission properties

Community Radiative Transfer Model

Support over 100 Sensors

- GOES-R ABI
- Metop IASI/HIRS/AVHRR/AMSU/MI
- TIROS-N to NOAA-18 AVHRR
- TIROS-N to NOAA-18 HIRS
- GOES-8 to 13 Imager channels
- GOES-8 to 13 sounder channel 08-13
- Terra/Aqua MODIS Channel 1-10
- MSG SEVIRI
- Aqua AIRS, AMSR-E, AMSU-A,HSB
- NOAA-15 to 18 AMSU-A
- NOAA-15 to 17 AMSU-B
- NOAA-18/19 MHS
- TIROS-N to NOAA-14 MSU
- DMSP F13 to15 SSM/I
- DMSP F13,15 SSM/T1
- DMSP F14,15 SSM/T2
- DMSP F16-20 SSMIS
- Coriolis Windsat
- TiROS-NOAA-14 SSU
- FY-3 IRAS, MWTS,MWHS,MWRI
- NPP/NPOESS CrIS/ATMS

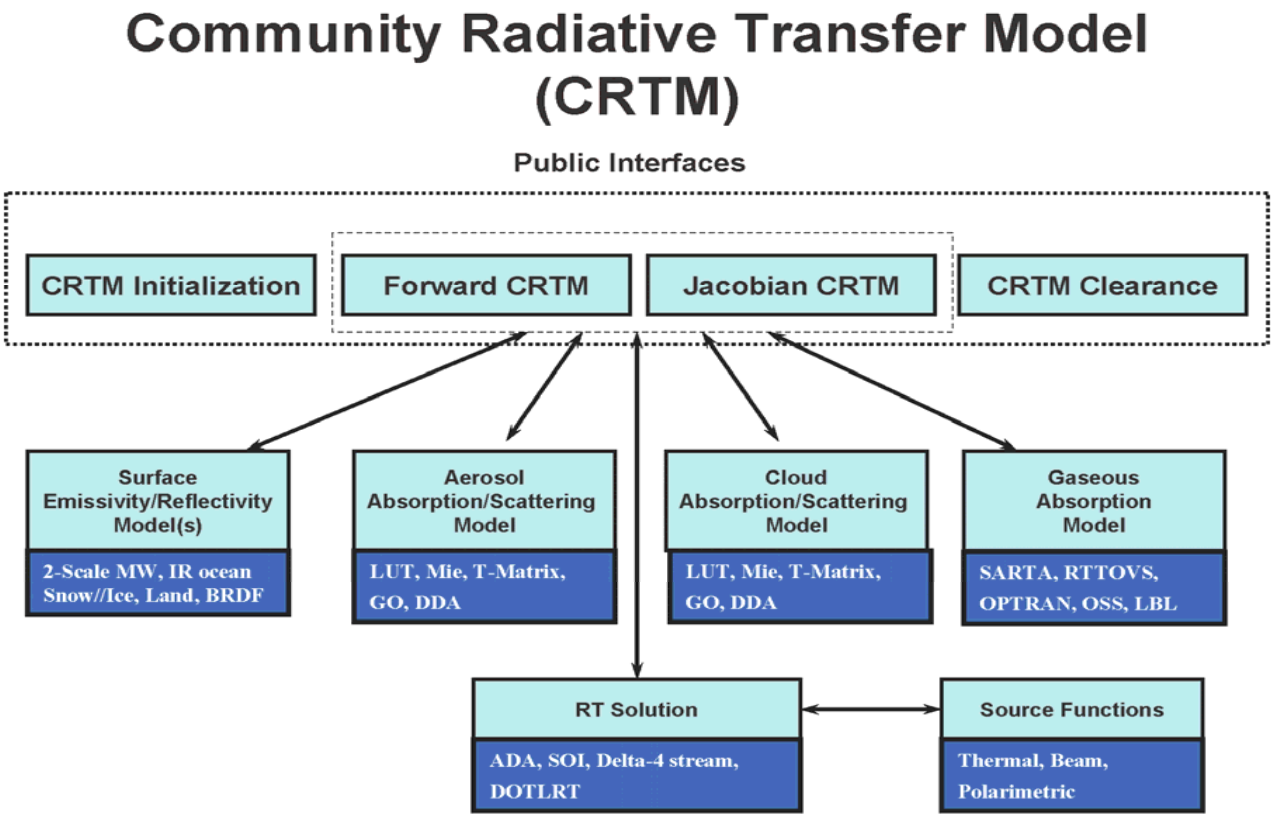

Radiative Transfer Schemes

- Emission-based
- Two (Four)-Stream Approximation
- Discrete Ordinate Method (DISORT)
- Advanced Doubling and Adding(ADA)
- Successive Order of Iteration (SOI)

Radiative Transfer Equation

1. Attenuation

2. Multiple Scattering

$$\mu \frac{d\mathbf{I}(\tau,\mu,\phi)}{d\tau} = -\mathbf{I}(\tau,\mu,\phi) + \frac{\omega(\tau)}{4\pi}\int_0^{2\pi}\int_{-1}^{1}\mathbf{M}(\tau,\mu,\phi;\mu',\phi')\mathbf{I}(\tau,\mu',\phi')d\mu' d\phi' + \mathbf{S}(\tau,\mu,\phi,\mu_0,\phi_0) \quad (3.8)$$

3. Source terms from thermal/solar

$$\mathbf{S}(\tau,\mu,\phi,\mu_0,\phi_0) = (1-\omega)B\begin{pmatrix}1\\0\\0\\0\end{pmatrix} + \frac{\omega F_0}{4\pi}\exp(-\tau/\mu_0)\begin{pmatrix}M_{11}(\phi,\mu_0,\phi_0)\\M_{12}(\phi,\mu_0,\phi_0)\\M_{13}(\phi,\mu_0,\phi_0)\\M_{14}(\phi,\mu_0,\phi_0)\end{pmatrix} \quad (3.9)$$

Emission-based Approach

3.3 Radiative Transfer Approximation

3.3.1 Emission-Based Model

Microwave radiative transfer can be simplified if single and multiple scattering terms are neglected and there is no azimuthally dependent terms are included. Thus, in Eq. 3.17, we can derive

$$\mu \frac{d\mathbf{I}(\tau,\mu)}{d\tau} = \mathbf{I}(\tau,\mu) - \mathbf{B}(\tau), \tag{3.21}$$

where $\mathbf{I}$ is the zeroth order term of radiance in the cosine mode in Eq.3.17. For convenience, we neglect the subscript of Fourier zeroth component. when the terms from single and multiple scattering are neglected and scattering. After the integration term disappears, the solution of radiance vector can be expressed in a form (Liou, 1980)

$$\begin{aligned} \mathbf{I}(\tau_0,\mu) &= \mathbf{I}(\tau_s,\mu)\exp(-\tau_s/\mu) + \\ &\int_0^1 \mathbf{r_s}(\mu,\mu')d\mu' \int_{\tau_0}^{\tau_s} \mathbf{B}(\tau,T)\exp[-\frac{(\tau-\tau_0)}{\mu'}]d\tau/\mu + \\ &\int_{\tau_s}^{\tau_0} \mathbf{B}(\tau,T)\exp[-\frac{(\tau_s-\tau)}{\mu}]d\tau/\mu, \end{aligned} \tag{3.22}$$

or

$$\begin{aligned} \mathbf{I}(\tau_0,\mu) &= \mathbf{I}(\tau_s,\mu)\exp(-\tau_s/\mu) + \mathbf{I_u} + \mathbf{I_d}, \qquad (3.23) \\ \mathbf{I_u} &= \int_{\tau_s}^{\tau_0} \mathbf{B}(\tau,T)\exp[-\frac{(\tau_s-\tau)}{\mu}]d\tau,/\mu \\ \mathbf{I_d} &= \int_0^1 \mathbf{r_s}(\mu,\mu')d\mu' \int_{\tau_0}^{\tau_s} \mathbf{B}(\tau,T)\exp[-\frac{(\tau-\tau_0)}{\mu'}]d\tau/\mu \end{aligned} \tag{3.24}$$

Emission-Based RT Model (1/3)

At the microwave frequencies, radiance is related to brightness temperature under Rayleigh-Jean approximation. Also, we only consider the first Stokes component (i.e. intensity), which is the brightness temperature. After some manipulation, we can derive

$$T_b = \epsilon T_s \exp(-\tau_s/\mu) + T_u + (1-\epsilon)(1+\Omega)(T_d + T_c)\exp(-\tau_s/\mu), \quad (3.25)$$

$$\begin{aligned} T_d &= \int_{\tau_0}^{\tau_s} B(\tau, T)\exp\left(-\frac{(\tau-\tau_0)}{\mu}\right) d\tau/\mu, \\ T_u &= \int_{\tau_s}^{\tau_0} B(\tau, T)\exp\left(-\frac{(\tau_s-\tau)}{\mu}\right) d\tau/\mu, \end{aligned} \quad (3.26)$$

where ϵ is the surface emissivity and T_s is the surface temperature, and T_c is the cosmic background brightness temperature. The parameter, Ω, is introduced for non-specular effect of surface reflection and varies with surface roughness, sea surface wind speed, frequency, and atmospheric transmittance (Wentz, 1998). Eq. 5.1 has been so far widely used for retrieving surface emissivity assume other components such as T_s, upwelling and downwelling brightness temperatures are estimated from other means (Weng et al., 2000; Prigent, 2004).

Emission-Based RT Model (2/3)

For an isothermal atmosphere, upwelling and downwelling components in terms of brightness temperatures can be approximated as

$$\begin{aligned} T_u &\approx T_d \\ &\equiv (1-\Upsilon)T_m, \end{aligned} \tag{3.27}$$

where $\Upsilon = \exp(-\frac{(\tau_s - \tau_0)}{\mu})$ and T_m is the atmospheric temperature. Thus,

$$T_b = T_s[1-(1-\epsilon)\Upsilon^2] - \Delta T(1-\Upsilon)[1+(1-\epsilon)\Upsilon], \tag{3.28}$$

where $\Delta T = T_s - T_m$. It is apparent that brightness temperatures under these approximation is directly related by the layer mean temperature and atmospheric transmittance. When emissivity is low (0.9), brightness temperature increases as atmospheric transmittance (more cloud and water vapor) decreases (see Fig. 3.3.1. This is why over oceans clouds having liquid water increases brightness temperature and are easily detected from lower microwave measurements. Eq. 5.4 can be analytically used to retrieve cloud liquid water path when ΔT is very small.

Emission-Based RT Model (3/3)

In an absence of scattering, brightness temperatures can be linearly a function of cloud liquid water path (L) and precipitable water path (V) (Weng et al. 2003) by further assuming an isothermal atmosphere in Eq. 5.4 and a Rayleigh scattering for liquid-phase droplets Eq. 3.44, i.e.,

$$T_b \quad = \quad T_s[1-(1-\epsilon)\Upsilon^2], \tag{6.1}$$

where ϵ and T_s are surface emissivity and temperature, respectively, and

$$\Upsilon = \exp[-(\tau_O + \tau_V + \tau_L)/\mu)] \tag{6.2}$$

where τ_O, τ_V and τ_L are the optical thicknesses of oxygen, water vapor and liquid respectively.

$$\tau_L = \int_{\Delta Z} \kappa^{Ray} LWC dz \tag{6.3}$$

where

$$\kappa^{Ray} = \frac{6\pi}{\lambda\rho_w} Im\left\{\frac{m^2-1}{m^2-2}\right\} \tag{6.4}$$

and

$$\tau_V = \int_0^\infty \kappa^{H_2O}\rho_V dz \tag{6.5}$$

where κ_{H_2O} is the mass absorption coefficient of water vapor having a unit of m^2/kg, and ρ_v is the water vapor density in atmosphere. Lets assume κ^{Ray} and κ^{H_2O} are independent of height. Then, we have

$$\tau_L = \kappa_L L \tag{6.6}$$

Discretization of Radiative Transfer Equation

$$\mathrm{I}(\tau,\mu,\phi) = \sum_{m=0}^{2N-1} [\mathrm{I}_m^c(\tau,\mu) cosm(\phi_0 - \phi) + \mathrm{I}_m^s(\tau,\mu) sinm(\phi_0 - \phi)], \qquad (3.13)$$

$$\mathrm{M}(\tau,\mu,\phi;\mu^{'},\phi^{'}) = \sum_{m=0}^{2N-1} [\mathrm{M}_m^c(\tau,\mu,\mu^{'}) cosm(\phi^{'} - \phi) + \mathrm{M}_m^s(\tau,\mu,\mu^{'}) sinm(\phi^{'} - \phi)].$$

$$\mathrm{S}(\tau,\mu,\phi) = \sum_{m=0}^{2N-1} [\mathrm{S}_m^c(\tau,\mu) cosm(\phi_0 - \phi) + \mathrm{S}_m^s(\tau,\mu) sinm(\phi_0 - \phi)], \qquad (3.16)$$

Discretization of Radiative Transfer Equation

$$\mu \frac{d\mathbf{I}_m^c(\tau,\mu)}{d\tau} = \mathbf{I}_m^c(\tau,\mu) - \frac{\omega(\tau)}{4}\int_{-1}^{1}[(1+\delta_{0m})\mathbf{M}_m^c\mathbf{I}_m^c - (1-\delta_{0m})\mathbf{M}_m^s\mathbf{I}_m^s]d\mu' - \mathbf{S}_m^c(\tau,\mu) \quad (3.17)$$

and

$$\mu \frac{d\mathbf{I}_m^s(\tau,\mu)}{d\tau} = \mathbf{I}_m^s(\tau,\mu) - \frac{\omega(\tau)}{4}\int_{-1}^{1}[(1-\delta_{0m})\mathbf{M}_m^c\mathbf{I}_m^s + (1-\delta_{0m})\mathbf{M}_m^s\mathbf{I}_m^c]d\mu' - \mathbf{S}_m^s(\tau,\mu), \quad (3.18)$$

$$m = 0, ..., (2N-1).$$

$$\mu_j \frac{d}{d\tau}\begin{pmatrix} \mathbf{I}(\tau,\mu_i) \\ \mathbf{I}(\tau,-\mu_i) \end{pmatrix} = -\begin{pmatrix} \mathbf{I}(\tau,\mu_i) \\ \mathbf{I}(\tau,-\mu_i) \end{pmatrix} + \omega\sum_{j=1}^{N} w_j \begin{pmatrix} \mathbf{M_m}(\mu_i,\mu_j) & \mathbf{M_m}(\mu_i,-\mu_j) \\ \mathbf{M_m}(-\mu_i,\mu_j) & \mathbf{M_m}(-\mu_i,-\mu_j) \end{pmatrix}\begin{pmatrix} \mathbf{I}(\tau,\mu_j) \\ \mathbf{I}(\tau,-\mu_j) \end{pmatrix} + \begin{pmatrix} \mathbf{S}(\tau,\mu_i) \\ \mathbf{S}(\tau,-\mu_i) \end{pmatrix} \quad (3.38)$$

Discrete Ordinate Method

$$
\mu_i \frac{dI(\tau,\mu_i)}{d\tau} = I(\tau,\mu_i) - \omega \sum_{j=1}^{N} w_j [P((\mu_i,\mu_j) I(\mu_j) + P((\mu_i,\mu_{-j}) I(\mu_{-j})] - (1-\omega)B(T) \tag{3.51}
$$

and

$$
\mu_{-i} \frac{dI(\tau,\mu_{-i})}{d\tau} = I(\tau,\mu_{-i}) - \omega \sum_{j=1}^{N} w_j [P((\mu_{-i},\mu_j) I(\mu_j) + P((\mu_{-i},\mu_{-j}) I(\mu_{-j})] - (1-\omega)B(T) \tag{3.52}
$$

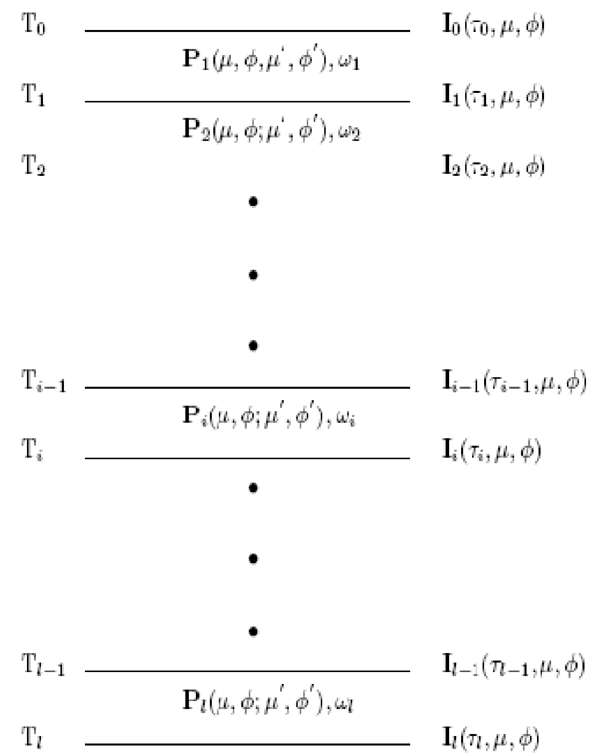

Figure 3.3: A schematic diagram of a multi-layer medium for the vector radiative transfer calculation. The temperature at each level is specified as known; the phase matrix, single scattering albedo and optical thickness at each layer are calculated from Mie theory. The radiative vector, including four radiative components, at each level, is calculated from the multi-layer discrete-ordinate method.

Scattering Approach: 2 Streams Approximation

3.3.2 Scattering-Based Model

For a scattering and absorbing atmosphere, the radiance may be considered azimuthally independent so that the radiative transfer equation is given as

$$\mu \frac{dI(\tau,\mu)}{d\tau} = I(\tau,\mu) - \frac{\omega(\tau)}{2}\int_{-1}^{1} P(\mu,\mu')I(\tau,\mu')d\mu' - (1-\omega(\tau))B(T) \quad (3.29)$$

where I is the radiance; $\omega(\tau)$ the single-scattering albedo; $P(\mu,\mu^{'})$ the phase function; $B(T)$ the Planck function; T the thermal temperature; τ the optical thickness; μ the cosine of incident zenith angle and $\mu^{'}$ the cosine of scattering zenith angle.

A solution for Eq. (??) was derived at arbitrary viewing angles using a two-stream approximation (Weng and Grody, 2000),

$$\mu \frac{dI(\tau,\mu)}{d\tau} = [1-\omega(1-b)]I(\tau,\mu) - \omega b I(\tau,-\mu) - (1-\omega)B, \quad (3.30)$$

$$-\mu \frac{dI(\tau,-\mu)}{d\tau} = [1-\omega(1-b)]I(\tau,-\mu) - \omega b I(\tau,\mu) - (1-\omega)B, \quad (3.31)$$

where b and $1-b$ is the ratio of the integrated scattering energy in the backward and forward directions, respectively. For an isotropic scattering, $b = 1/2$ so that the scattered energy is the same in both directions. Since b is generally less than $1/2$, forward scattering is much stronger than backward scattering and the resulting upwelling radiation is reduced.

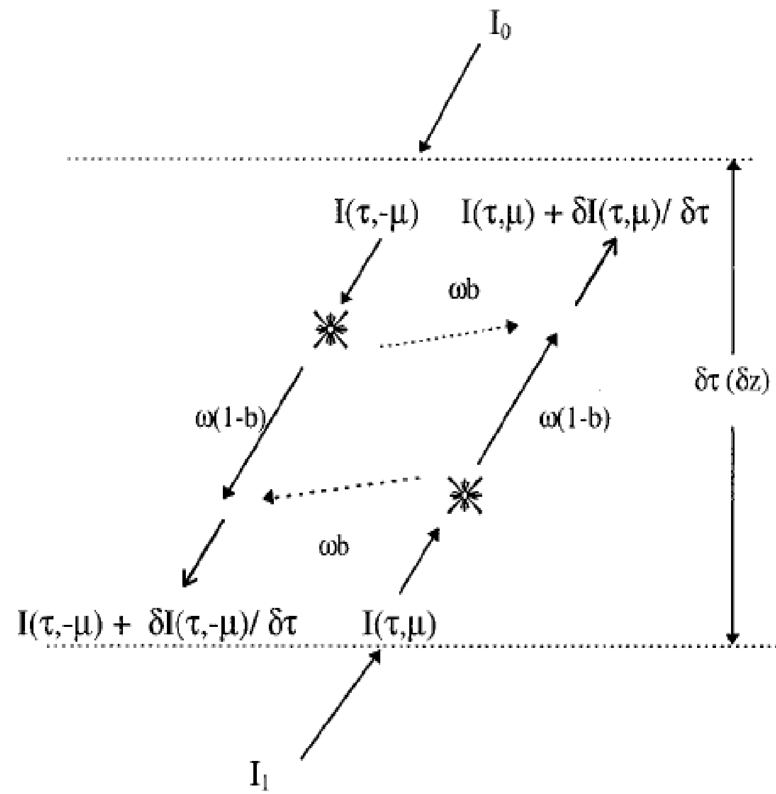

FIG. 1. A schematic diagram of the two-stream radiative transfer in an ice cloud layer.

Two-Stream Model Solution

Equations (3.30) and (3.31) can be combined into two decoupled second order differential equations with constant coefficients, assuming that ω, b and B are independent of τ. These equations can be used to analyze the scattering from the atmosphere or surface. The upwelling radiance observed from satellites for an ice cloud layer is derived by neglecting reflections at the cloud top and bottom (Weng and Grody, 2000). However, for surfaces such as snow, the upwelling radiance is modified by the reflectivity and transmissivity at the upper boundary where a discontinuity in the dielectric constant occurs (see Fig. 1). As a result, the solutions for the upwelling and downwelling radiance are

$$I(\tau,\mu) = \frac{I_0'[\gamma_1 e^{\kappa(\tau-\tau_1)} - \gamma_2 e^{-\kappa(\tau-\tau_1)}] - I_1'[\beta_3 e^{\kappa(\tau-\tau_0)} - \beta_4 e^{-\kappa(\tau-\tau_0)}]}{\beta_1\gamma_4 e^{-\kappa(\tau_1-\tau_0)} - \beta_2\gamma_3 e^{\kappa(\tau_1-\tau_0)}} + B \tag{3.32}$$

$$I(\tau,-\mu) = \frac{I_0'[\gamma_4 e^{\kappa(\tau-\tau_1)} - \gamma_3 e^{-\kappa(\tau-\tau_1)}] - I_1'[\beta_2 e^{\kappa(\tau-\tau_0)} - \beta_1 e^{-\kappa(\tau-\tau_0)}]}{\beta_1\gamma_4 e^{-\kappa(\tau_1-\tau_0)} - \beta_2\gamma_3 e^{\kappa(\tau_1-\tau_0)}} + B \tag{3.33}$$

where κ is the eigenvalue in solving the differential equations and related to particle optical parameters. Also, $I_1' = I_1 - B(1 - R_{23})$; $I_0' = I_0(1 - R_{12}) - B(1 - R_{21})$, where I_1 is the upwelling radiance at $\tau = \tau_1$ from the bottom layer and I_0 is the downwelling radiance at $\tau = \tau_0$ from the top layer. The

Advanced Doubling-Adding (ADA)
Liu and Weng, 2006, JAS

1. Compute layer transmission and reflection (loop i from 0→ n-1)

$$\mathbf{r}(\delta_0) = \delta_0 \boldsymbol{\beta} \qquad \mathbf{t}(\delta_0) = \mathbf{E} + \boldsymbol{\alpha}\delta_0 \qquad \delta = \delta_n = 2^n \delta_0$$

$$\mathbf{r}(\delta_{i+1}) = \mathbf{t}(\delta_i)[\mathbf{E} - \mathbf{r}(\delta_i)\mathbf{r}(\delta_i)]^{-1}\mathbf{r}(\delta_i)\mathbf{t}(\delta_i) + \mathbf{r}(\delta_i) \qquad \mathbf{t}(\delta_{i+1}) = \mathbf{t}(\delta_i)[\mathbf{E} - \mathbf{r}(\delta_i)\mathbf{r}(\delta_i)]^{-1}\mathbf{t}(\delta_i)$$

2. Compute layer source functions

$$\mathbf{S_u} = [(\mathbf{E} - \mathbf{t} - \mathbf{r})B(T_1) - (B(T_2) - B(T_1))\mathbf{t} + \frac{B(T_2) - B(T_1)}{(1 - \varpi g)\delta}(\mathbf{E} + \mathbf{r} - \mathbf{t})\mathbf{u}]\boldsymbol{\Xi} + \frac{\varpi F_0}{\pi}\exp(-\frac{\tau_{k-1}}{\mu_0})[(\mathbf{E} - \mathbf{t}\exp(-\frac{\delta}{\mu_0}))\Psi_u - \mathbf{r}\Psi_d]$$

$$\mathbf{S_d} = [(\mathbf{E} - \mathbf{t} - \mathbf{r})B(T_1) + (B(T_2) - B(T_1))(\mathbf{E} - \mathbf{r}) + \frac{B(T_2) - B(T_1)}{(1 - \varpi g)\delta}(\mathbf{t} - \mathbf{E} - \mathbf{r})\mathbf{u}]\boldsymbol{\Xi} + \frac{\varpi F_0}{\pi}\exp(-\frac{\tau_{k-1}}{\mu_0})[(\exp(-\frac{\delta}{\mu_0})E - \mathbf{t})\Psi_d - \mathbf{r}\exp(-\frac{\delta}{\mu_0})\Psi_u]$$

$$\begin{bmatrix} \Psi_d \\ \Psi_u \end{bmatrix} = -\frac{\varpi F_\lambda}{(1+\delta_{0m})\pi}\begin{bmatrix} \boldsymbol{\alpha} + E/\mu_0 & \boldsymbol{\beta} \\ -\boldsymbol{\beta} & -\boldsymbol{\alpha} + E/\mu_0 \end{bmatrix}^{-1}\begin{bmatrix} \phi(\mu_i, \mu_0) \\ \phi(-\mu_i, \mu_0) \end{bmatrix}$$

3. Vertical integration

$$\mathbf{I_u}(n) = \varepsilon B(T_s) + \frac{F_\lambda \exp(-\tau_N/\mu_0)}{(1+\delta_{0m})\pi}R_s(\mu_0)$$

$\mathbf{R}(n)$ the surface reflection matrix, loop k from n → 1

$$\begin{aligned}\mathbf{I_u}(k-1) &= \mathbf{S_u}(k) + \mathbf{t}(k)[\mathbf{E} - \mathbf{R}(k)\mathbf{r}(k)]^{-1}\ \mathbf{R}(k)\mathbf{S_d}(k) + \mathbf{t}(k)[\mathbf{E} - \mathbf{R}(k)\mathbf{r}(k)]^{-1}\ \mathbf{I_u}(k) \\ &= \mathbf{S_u}(k) + \mathbf{t}(k)[\mathbf{E} - \mathbf{R}(k)\mathbf{r}(k)]^{-1}\ [\mathbf{R}(k)\mathbf{S_d}(k) + \mathbf{I_u}(k)]\end{aligned}$$

$$\mathbf{R}(k-1) = \mathbf{r}(k) + \mathbf{t}(k)[\mathbf{E} - \mathbf{R}(k)\mathbf{r}(k)]^{-1}\ \mathbf{R}(k)\mathbf{t}(k)$$

4. Final TOA radiance

$$\mathbf{R}adiance = \mathbf{I}_u(0) + \mathbf{R}(0)\mathbf{I}_{sky}$$

Doubling & Adding

For an infinitesimal optical depth δ_0, multiple scattering can be neglected and the reflection matrix can be expressed as (Plass et al. 1973)

$$\mathbf{r}(\delta_0) = \delta_0 \boldsymbol{\beta}, \tag{6a}$$

and the transmission matrix can be written as

$$\mathbf{t}(\delta_0) = \mathbf{E} + \boldsymbol{\alpha}\delta_0, \tag{6b}$$

where $\mathbf{E}$ is an $N \times N$ unit matrix.

Using the doubling procedure from Van de Hulst (1963), the reflection and transmission matrices for a finite optical depth ($\delta = \delta_n = 2^n \delta_0$) can be computed by doubling the optical depth (i.e., $\delta_{i+1}/\delta_i = 2$) recursively:

$$\mathbf{r}(\delta_{i+1}) = \mathbf{t}(\delta_i)[\mathbf{E} - \mathbf{r}(\delta_i)\mathbf{r}(\delta_i)]^{-1}\mathbf{r}(\delta_i)\mathbf{t}(\delta_i) + \mathbf{r}(\delta_i), \tag{7a}$$

and

$$\mathbf{t}(\delta_{i+1}) = \mathbf{t}(\delta_i)[\mathbf{E} - \mathbf{r}(\delta_i)\mathbf{r}(\delta_i)]^{-1}\mathbf{t}(\delta_i), \tag{7b}$$

for $i = 0, n-1$. We denote $\mathbf{r}(k) = \mathbf{r}(\delta_n)$ and $\mathbf{t}(k) = \mathbf{t}(\delta_n)$ for the reflection and transmission matrices of kth layer.

Atmospheric Gaseous Absorption Line by Line Calculation

- The absorption coefficient is a complicated and highly non-linear function
- Line Strengths, Sij, result from many molecular vibrational-rotational transitions.

$$\kappa_i(\nu, p, T, \theta) \simeq \sum_{j=1}^{J} \frac{N_i \cdot S_{ij}}{\pi} \frac{\gamma_{ij}}{(\nu - \nu_{ij})^2 + (\gamma_{ij})^2} \cdot \sec(\theta)$$

$$\gamma_{ij} \simeq \gamma_{ij}^0 \cdot \frac{p}{P_0} \cdot \sqrt{\frac{T}{T_0}}$$

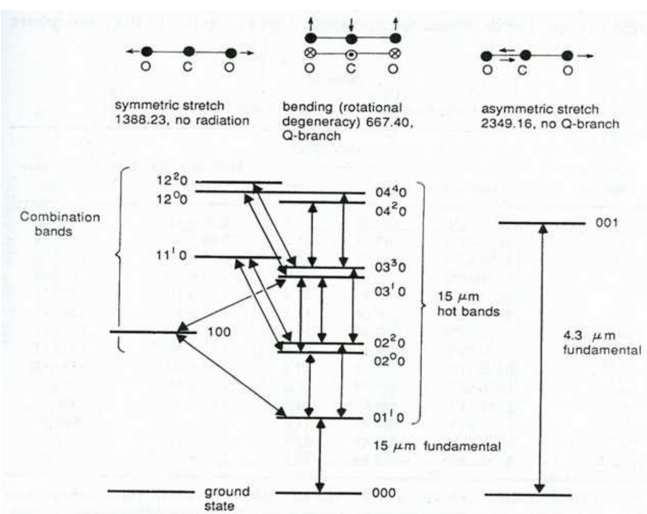

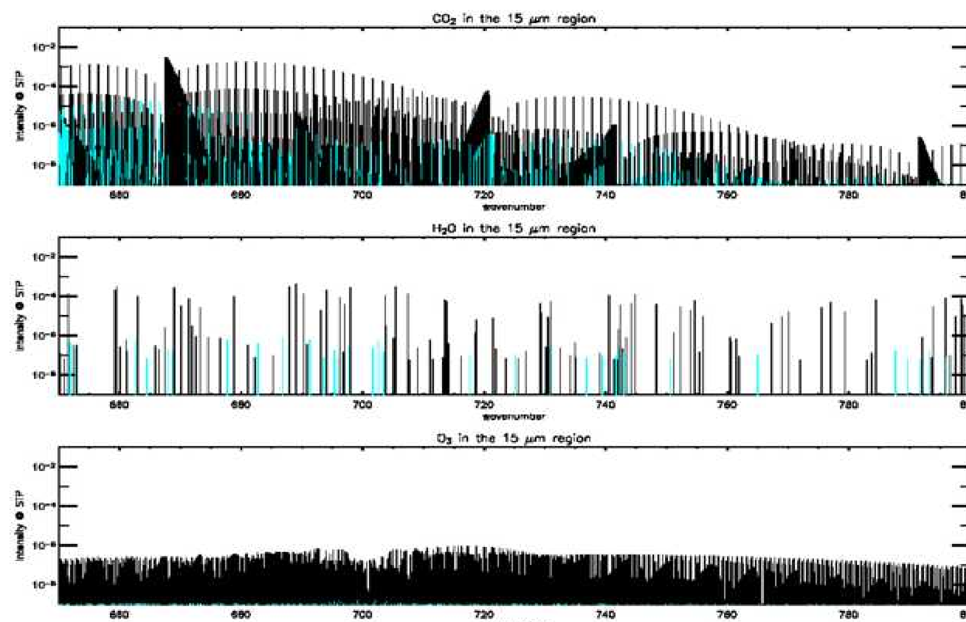

Fast Gaseous Absorption Algorithms (1/2)

For simplicity, let the index i represent water vapor, ozone or dry gas and $\mathrm{T}_{ch,i}(A_i)$ one of the three transmittance components, $\mathrm{T}_{ch,w}$, $\mathrm{T}^*_{ch,d}$ and $\mathrm{T}^*_{ch,o}$, at the level with the integrated absorber amount A_i (from space to the pressure level p), which is computed as

$$A_i = \int_0^p \frac{r_i}{g\cos(\theta)} dp' , \qquad (8)$$

where r_i is the gas specific amount, θ the zenith angle and g the gravitation constant. With the symbols defined, the transmittance is calculated as

$$\mathrm{T}_{ch,i}(A_i) = e^{-\int_0^{A_i} k_{ch,i}(A_i')dA_i'} , \qquad (9)$$

where

$$Ln(k_{ch,i}(A_i)) = c_{i,0}(A_i) + \sum_{j=1}^{6} c_{i,j}(A_i)x_{i,j}(A_i) ,$$

In (9), $k_{ch,i}(A_i)$ is the absorption coefficient and $Ln()$ is the natural logarithm. The predictors $x_{i,j}(A_i)$ ($j = 1, 6$) are functions of atmospheric state variables and the coefficients $c_{i,0}(A_i)$ and $c_{i,j}(A_i)$ are polynomial functions of A_i in the form:

$$c_{i,j}(A_i) = \sum_{n=0}^{N} a_{i,j,n} Ln(A_i)^n , \qquad (10)$$

Fast Gaseous Absorption Algorithms (2/2)

Table 1 Standard and integrated predictors

Standard Predictors		Integrated predictors			
1	T	1	T_w*	12	P_o***
2	P	2	T_w**	13	T_d*
3	T^2	3	T_w***	14	T_d**
4	P^2	4	P_w*	15	T_d***
5	$T\,P$	5	P_w**	16	P_d*
6	$T^2\,P$	6	P_w***	17	P_d**
7	$T\,P^2$	7	T_o*	18	P_d***
8	$T^2\,P^2$	8	T_o**		
9	$\sqrt[4]{P}$	9	T_o***		
10	Q	10	P_o*		
11	$Q/\sqrt{T}$	11	P_o**		

- see equation 11 for their definition
- T – temperature; P – pressure

CRTM Fast Gaseous Absorption Models

Version 1 performance:
Variable gases: H2O, O3
Fixed gas: CO2, CO, CH4, N2O, O2

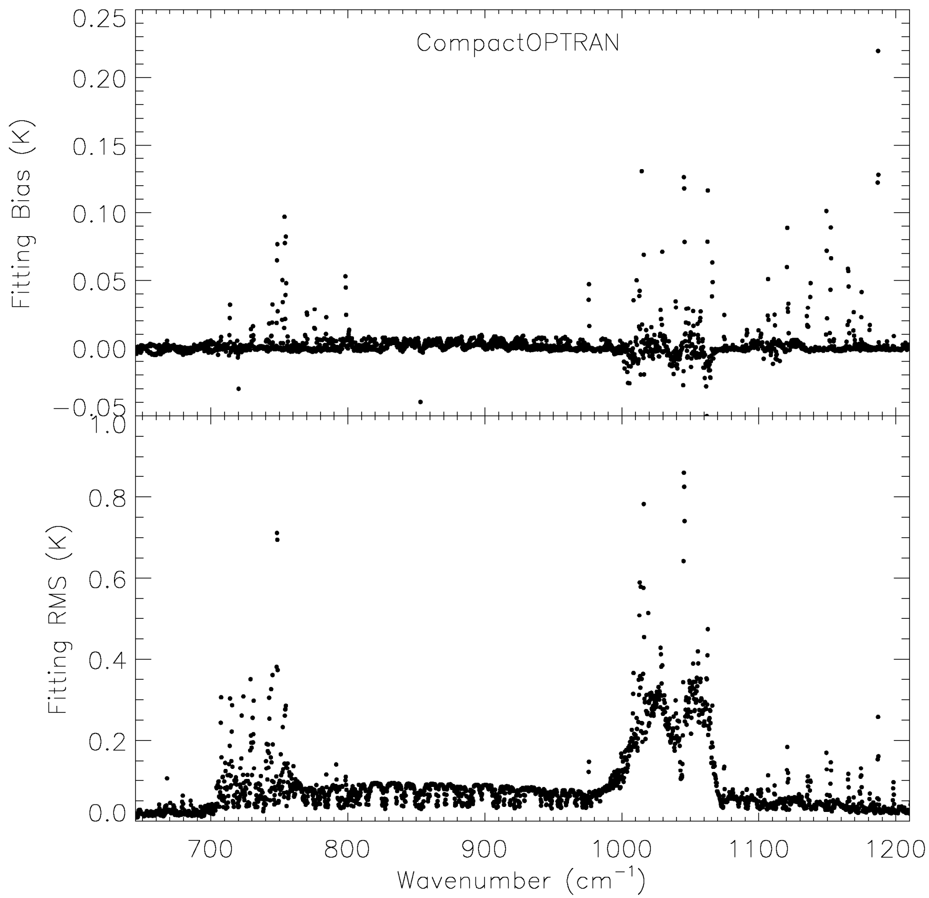

Version 2 performance
Variable gases: CO2, H2O, O3
Fixed gas: CO, CH4, N2O, O2, CFCs and others

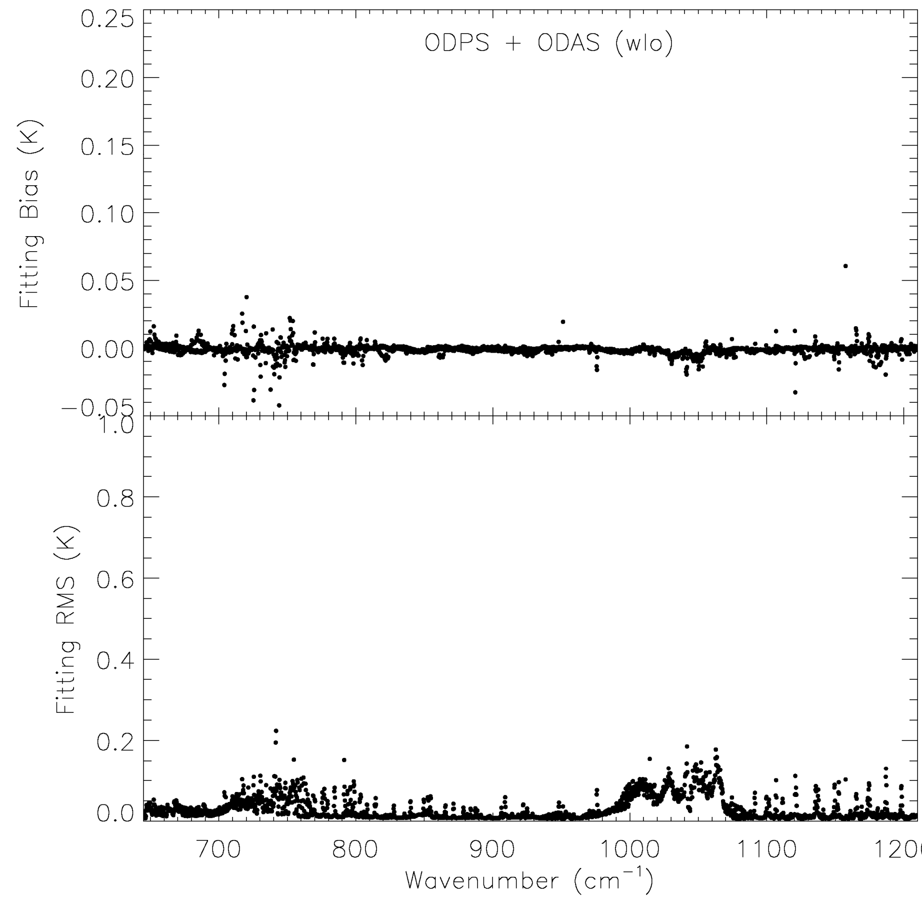

Microwave LBL (MonoRTM) Data Base

- Update to MT_CKD water vapor continuum in microwave
  - Based on ARM ground-based radiometer data
  - Preliminary numbers for changes:
    - ~10 % decrease in foreign
    - ~20 % increase in self
- Additional features:
  - Extension beyond microwave region
  - Improved consistency with LBLRTM in terms of coding and databases

Improvement of Infrared LBL Data Base

LBLRTM

CO_2 line parameters

Tashkun et al. (1999)

CO_2 line coupling

Application of Niro et al. (2005) code to Tashkun line parameters

CO_2 continuum

Using ARM ground-based interferometer meas.

H_2O line parameters

Coudert et al. (2008)

Updates to LBLRTM are all independent of the AIRS dataset used here to demonstrate them.

MonoRTM

H_2O continuum

Using ARM ground-based radiometer meas. (Payne et al., 2009, in preparation)

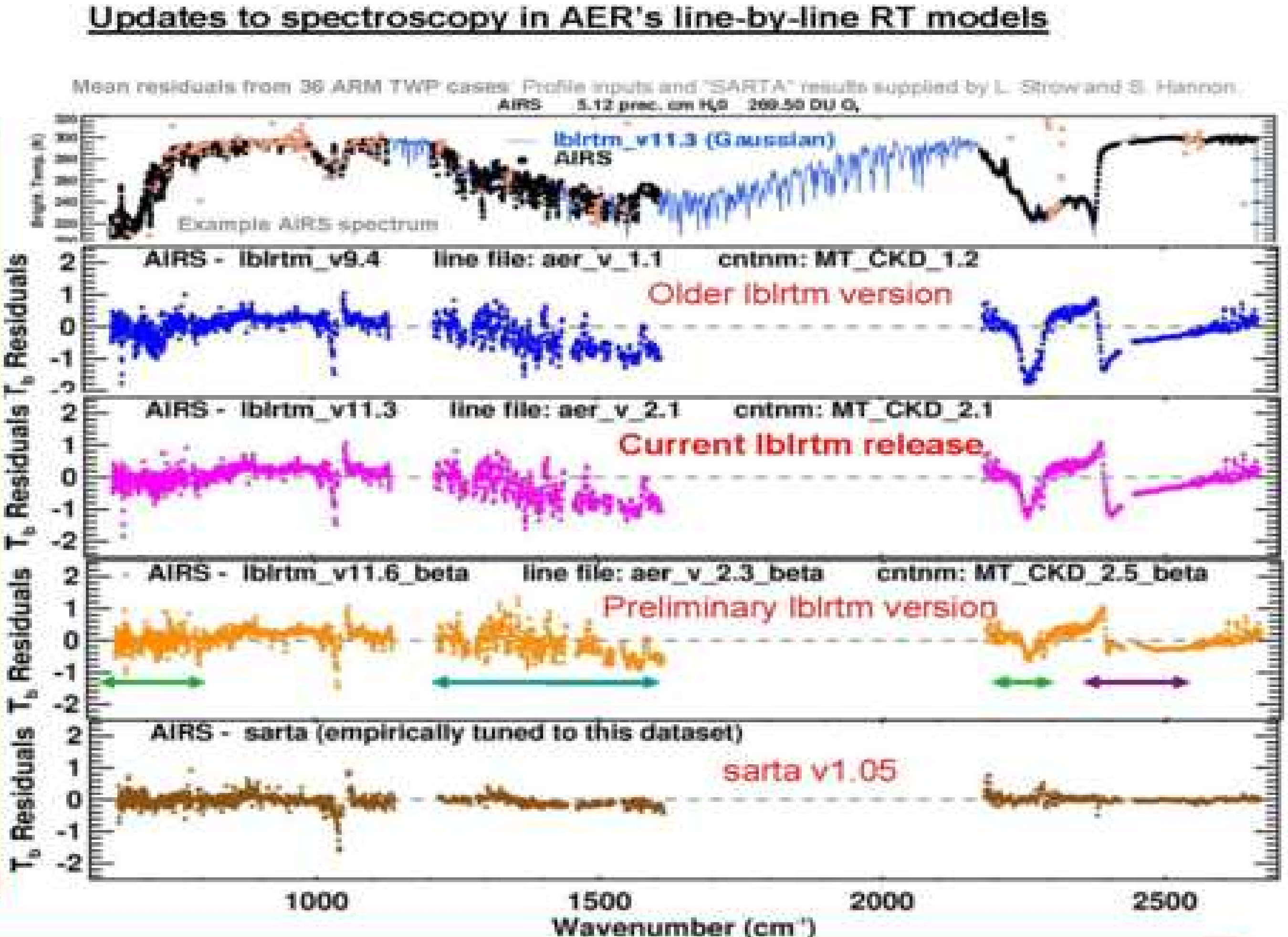

Significant improvements to consistency between spectral regions!

Zeeman Effects in CRTM

Energy level splitting:

In the presence of an external magnetic field, each energy level associated with the total angular momentum quantum number J is split into 2J+1 levels corresponding to the azimuthal quantum number M = -J, …, 0, …,J

Transition lines (Zeeman components) :

The selection rules permit transitions with $\Delta J = \pm 1$ and $\Delta M = 0, \pm 1$. For a change in J (i.e. J=3 to J=4, represented by 3^+), transitions with

- $\Delta M = 0$ are called π components,
- $\Delta M = 1$ are called σ+ components and
- $\Delta M = -1$ are called σ- components.

Polarization:

The three groups of Zeeman components also exhibit polarization effects with different characteristics. Radiation from these components received by a circularly polarized radiometer such as the SSMIS upper-air channels is a function of the magnetic field strength |**B**|, the angle θ_B between **B** and the wave propagation direction **k** as well as the state of atmosphere, not dependent on the azimuthal angle of **k** relative to **B**.

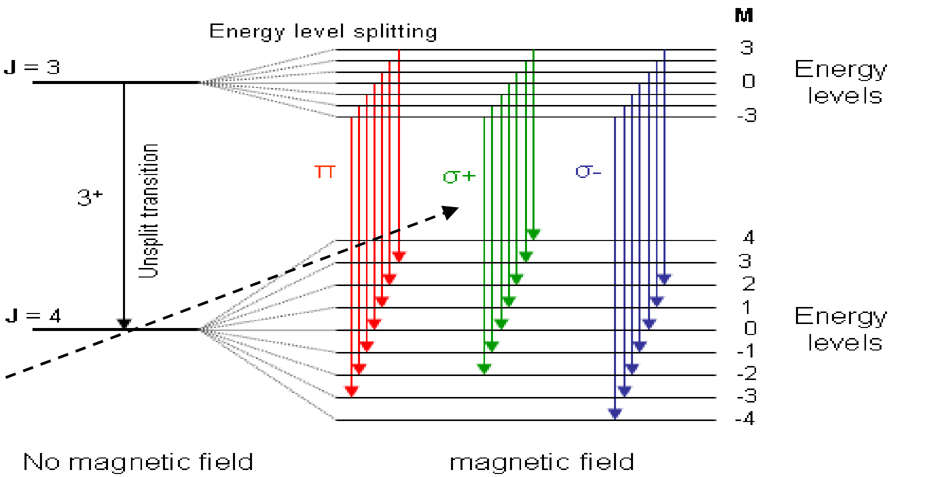

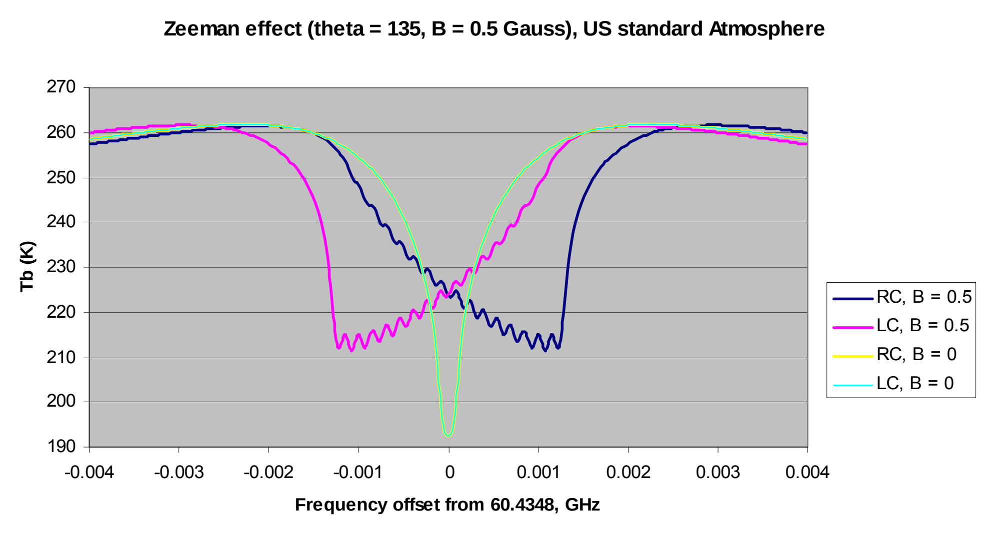

SSMIS Zeeman Splitting Related Errors

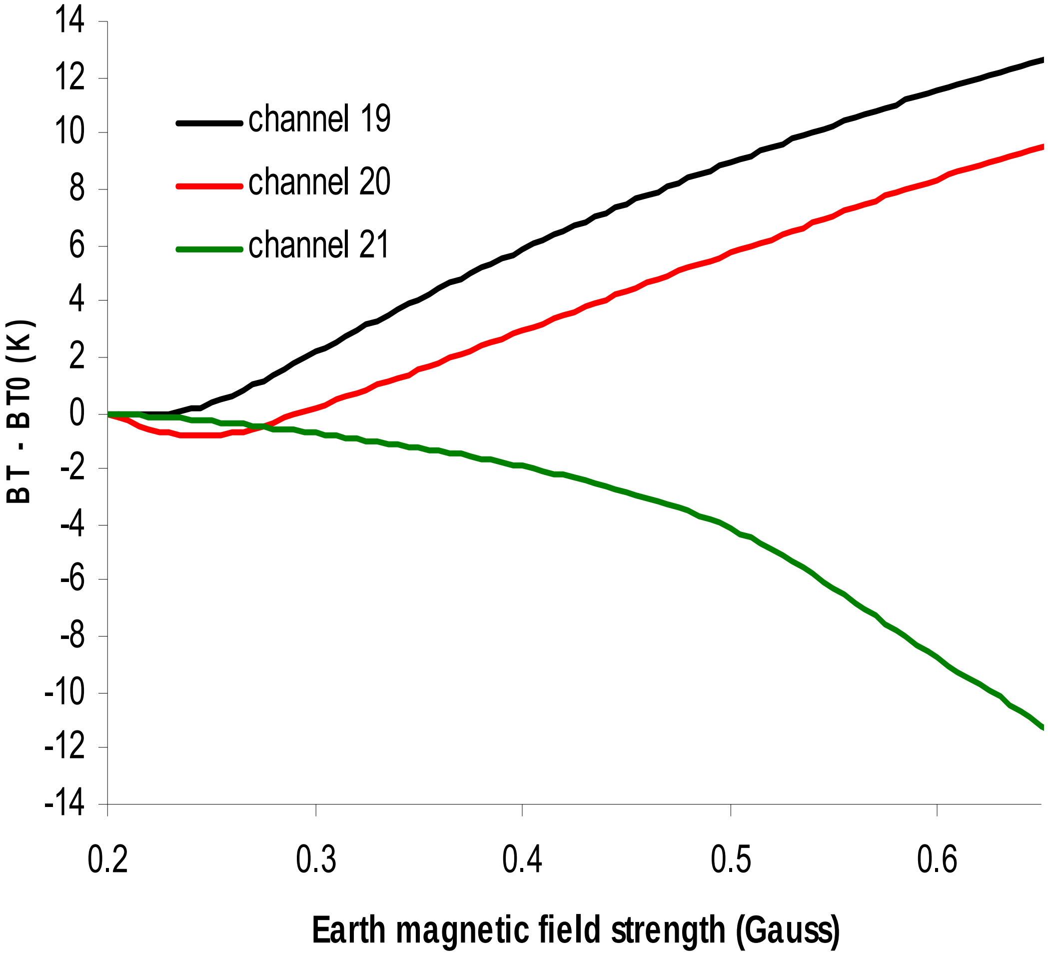

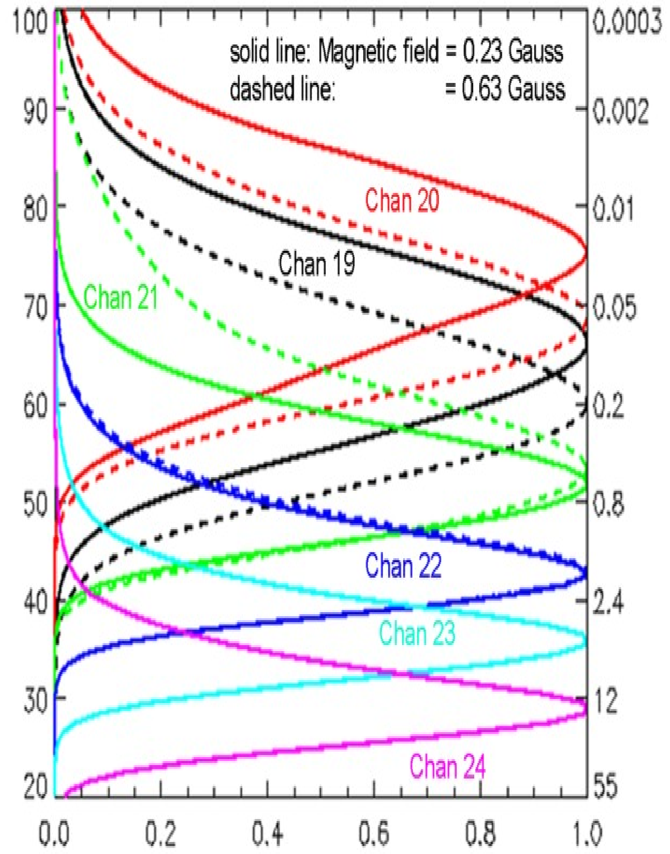

Fast Zeeman Absorption Model

(1) Atmosphere is vertically divided into N fixed pressure layers from 0.000076 mb (about 110km) to 200 mb. (currently N=100, each layer about 1km thick).

(2) The Earth's magnetic field is assumed constant vertically

(3) For each layer, the following regression is applied to derive channel optical depth with a left-circular polarization:

$$\tau_i = \tau_{i-1} \exp(-OD_{lc,i} / COS(\theta)), \quad \tau_0 = 1$$

$$OD_{lc,i} = c_{i,0} + \sum_{j=1}^{m} c_{i,j} x_{i,j}$$

ψ – 300/T; T – temperature
B – Earth magnetic field strength
θ_B – angle between magnetic field and propagation direction

SSMIS UAS Simulated vs. Observed

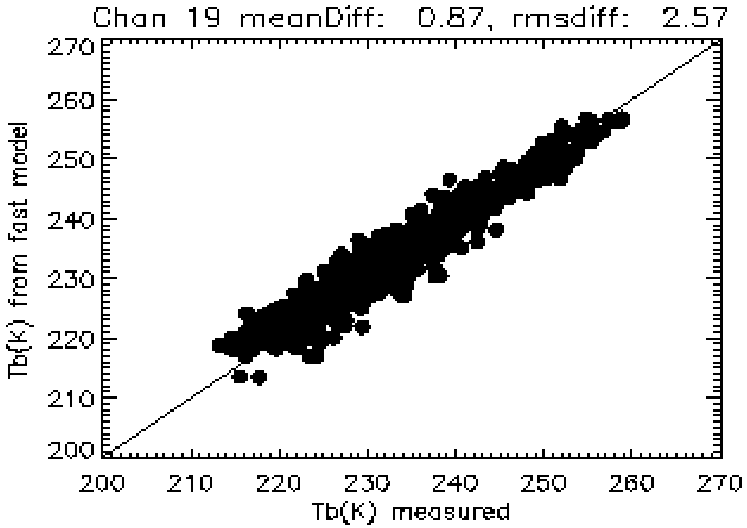

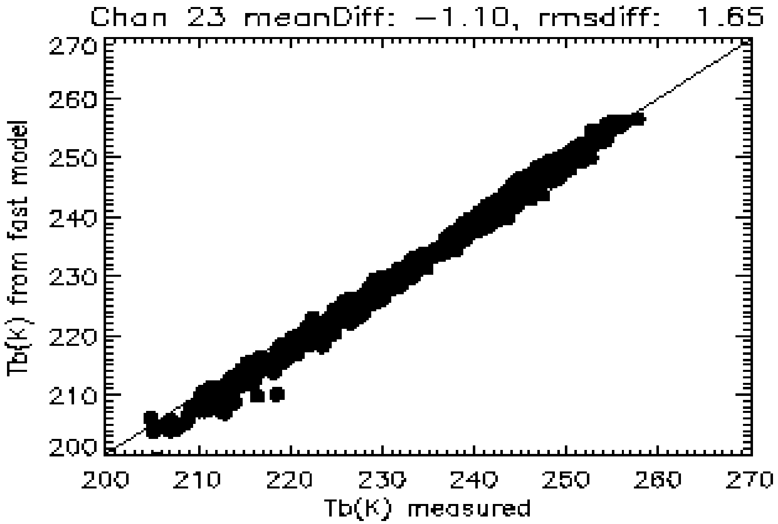

From Han, 2006, 15th ITSC

AMSU-A channel-14 brightness temperature differences between RT models w/o Zeeman-splitting effect

Model inputs:

B_e, θ_e, Φ_e – calculated using IGRF10 and data from AMSU-A MetOp-a 1B data files on September 8, 2007.

Atmospheric profile – US standard atmosphere applied over all regions.

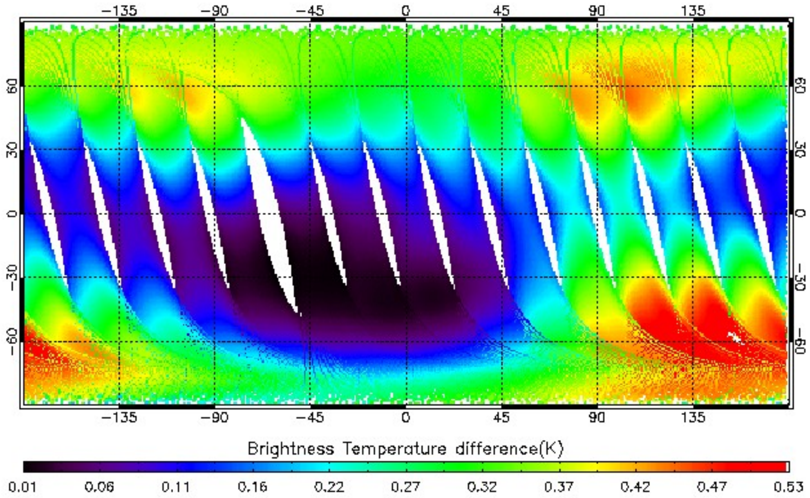

Ascending

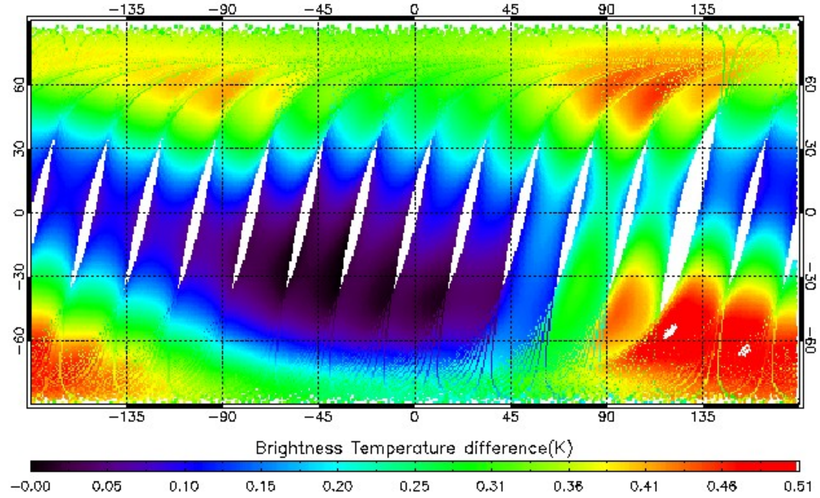

Descending

Cloud Scattering Properties (1/2)

$$De = \frac{3\int_{L_{\min}}^{L_{\max}} V(L)n(L)dL}{2\int_{L_{\min}}^{L_{\max}} A(L)n(L)dL}, \quad (2)$$

$$\langle Q_e \rangle = \frac{\int_{L_{\min}}^{L_{\max}} Q_e(L)A(L)n(L)dL}{\int_{L_{\min}}^{L_{\max}} A(L)n(L)dL}, \quad (3)$$

$$\langle Q_a \rangle = \frac{\int_{L_{\min}}^{L_{\max}} Q_a(L)A(L)n(L)dL}{\int_{L_{\min}}^{L_{\max}} A(L)n(L)dL}, \quad (4)$$

$$\langle g \rangle = \frac{\int_{L_{\min}}^{L_{\max}} g(L)Q_s(L)A(L)n(L)dL}{\int_{L_{\min}}^{L_{\max}} Q_s(L)A(L)n(L)dL}, \quad (5)$$

$$\langle \omega \rangle = \frac{\int_{L_{\min}}^{L_{\max}} Q_s(L)A(L)n(L)dL}{\int_{L_{\min}}^{L_{\max}} Q_e(L)A(L)n(L)dL}, \quad (6)$$

$$\langle P11(\Theta) \rangle = \frac{\int_{L_{\min}}^{L_{\max}} P11(\Theta,L)Q_s(L)A(L)n(L)dL}{\int_{L_{\min}}^{L_{\max}} Q_s(L)A(L)n(L)dL}, \quad (7)$$

$$\langle f \rangle = \frac{\int_{L_{\min}}^{L_{\max}} f(L)Q_s(L)A(L)n(L)dL}{\int_{L_{\min}}^{L_{\max}} Q_s(L)A(L)n(L)dL}, \quad (8)$$

where De is particle effective size, V is particle volume, A is the projected area, Qe is extinction efficiency, Qa is the absorption efficiency, g is the asymmetry factor, ω is the single-scattering albedo, P11 is the single-scattering phase function, and the factor f is associated with δ transmission of the incident rays through two parallel faces of the scattering particle.

$$n(L) = N_0 L^{\mu} \exp\left(\frac{b+\mu+0.67}{L_m} L\right), \quad (1)$$

where N_0 is the intercept, μ is the dispersion (usually ranging from 0 to 2, assumed to be

Cloud Scattering Properties (2/2)

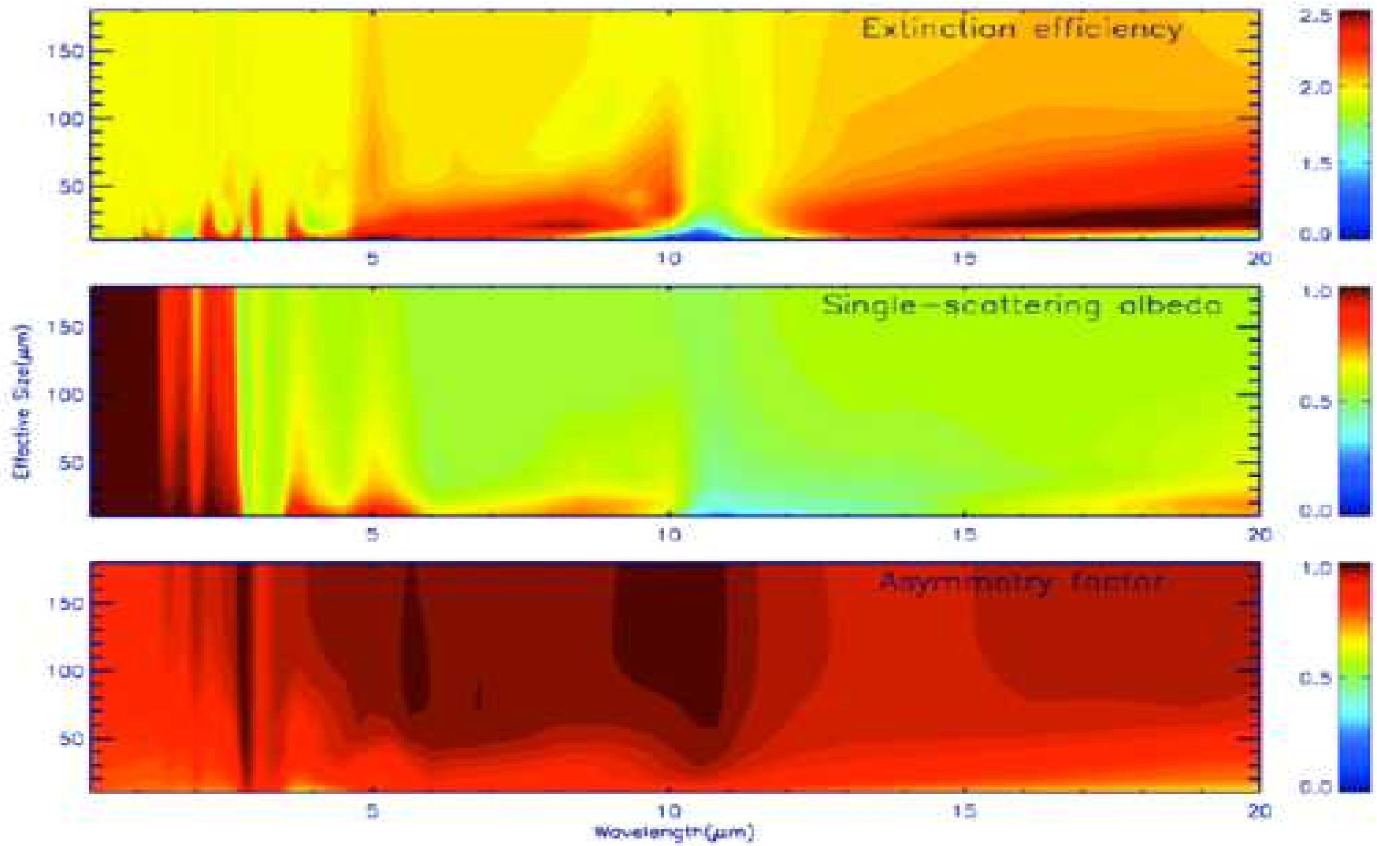

Fig. 1. Contours of the extinction efficiency, single-scattering albedo and asymmetry factor as functions of wavelength and effective particle size for ice crystals.

Infrared Properties of Clear Skies & Cirrus

CO_2 Slicing Bands

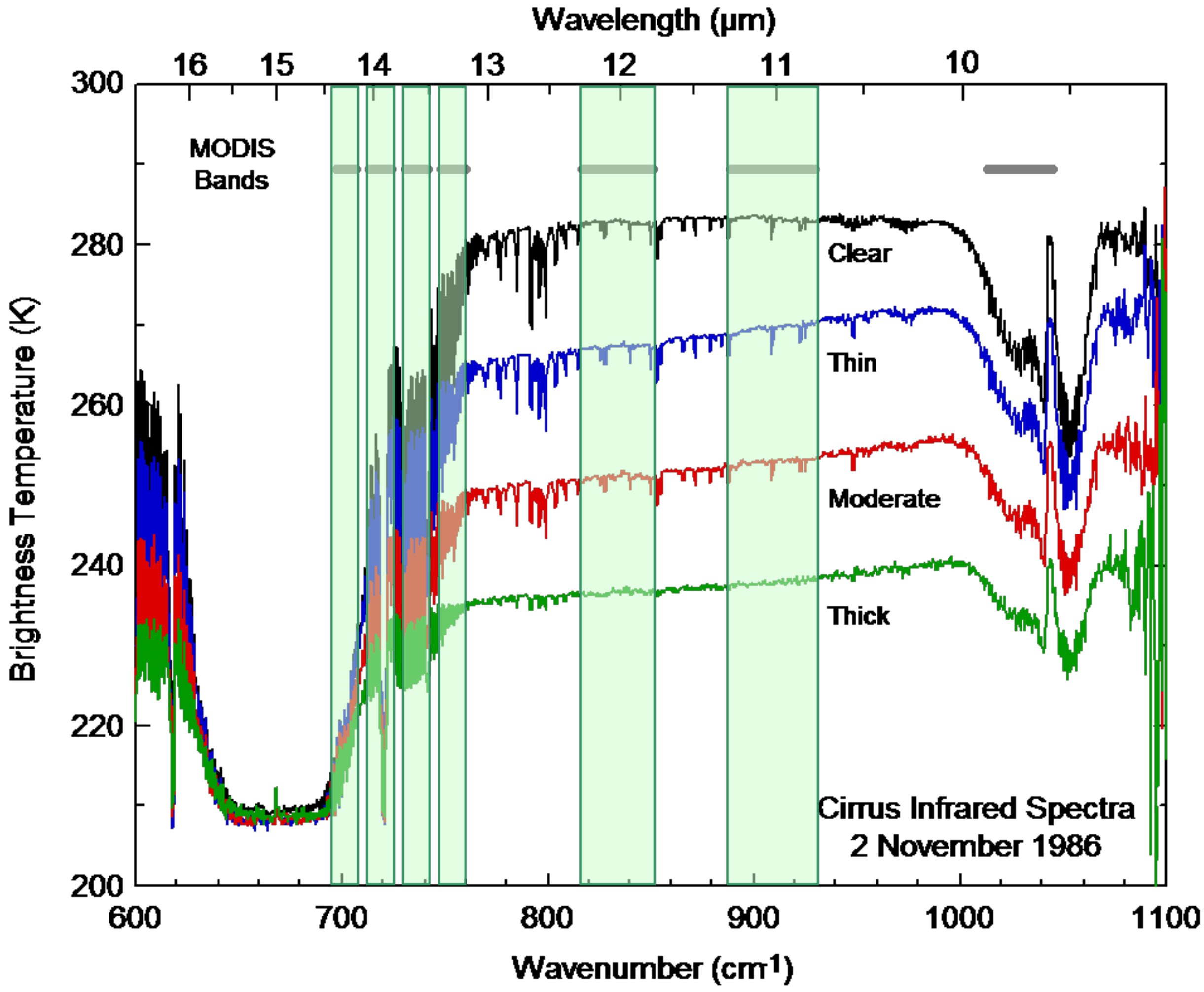

Shortwave Properties of Clouds
Cloud Mask Bands

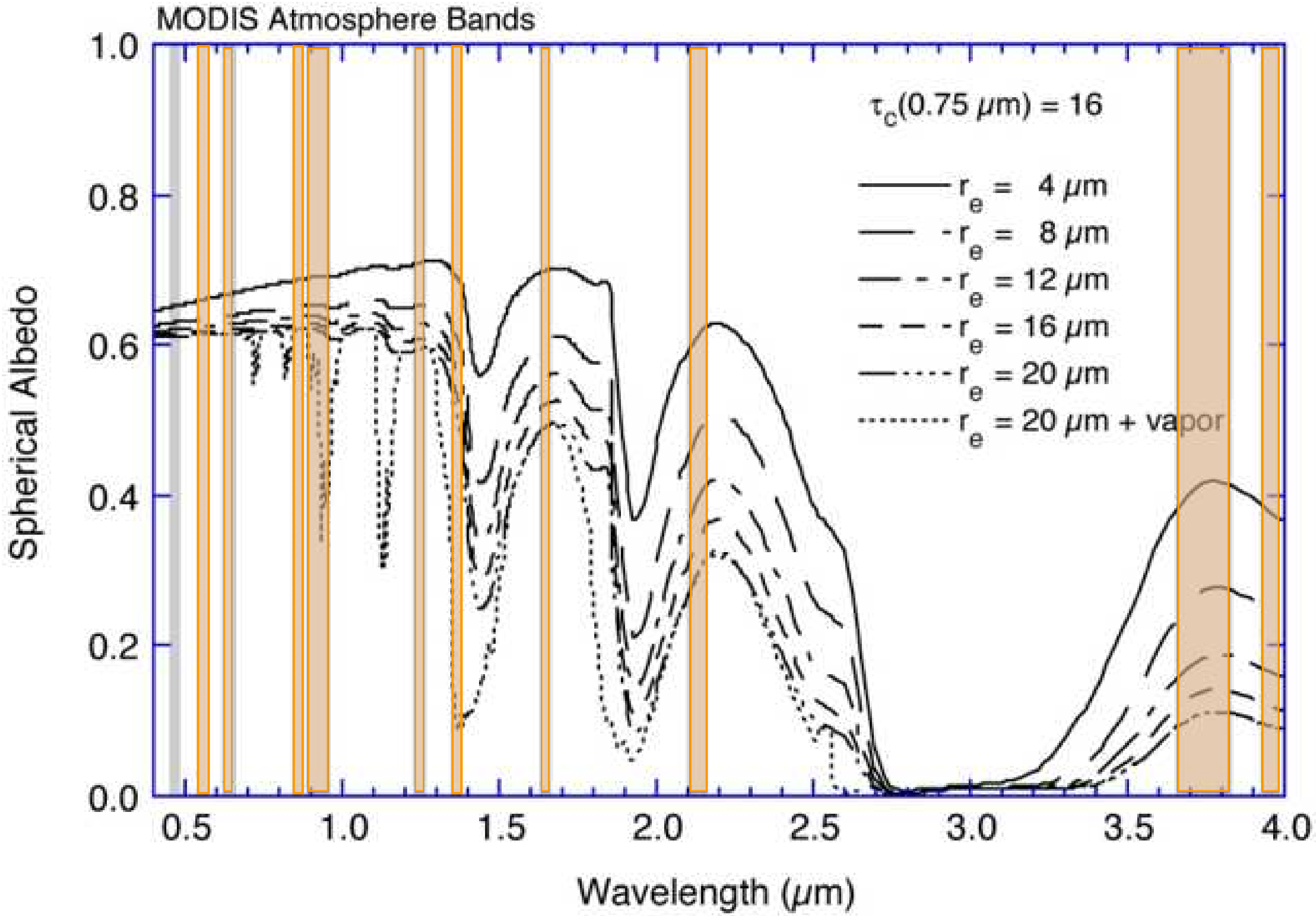

Infrared Properties of Clouds
Cloud Mask Bands

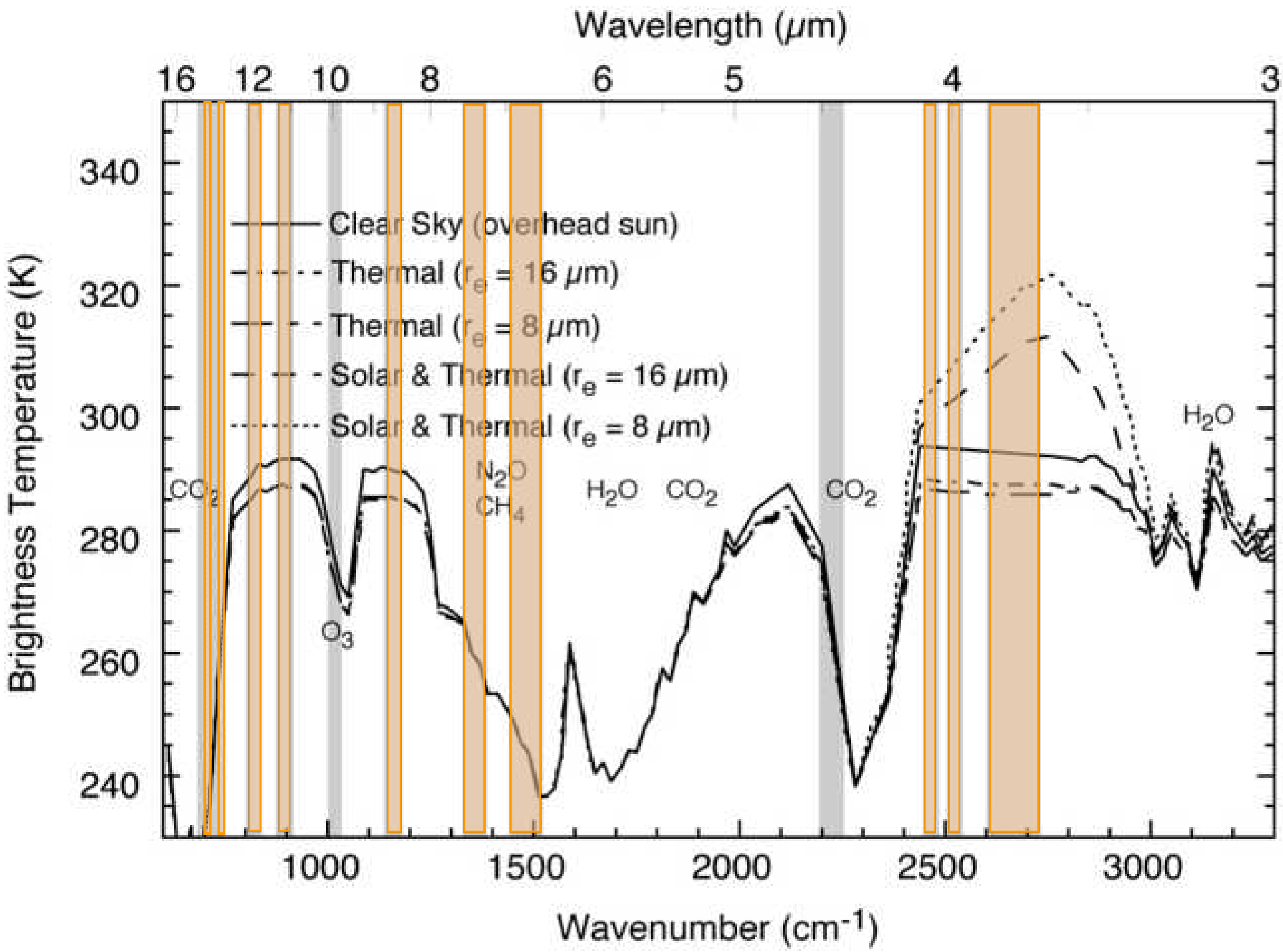

Ice Cloud Model Used for the CRTM

Habit distribution

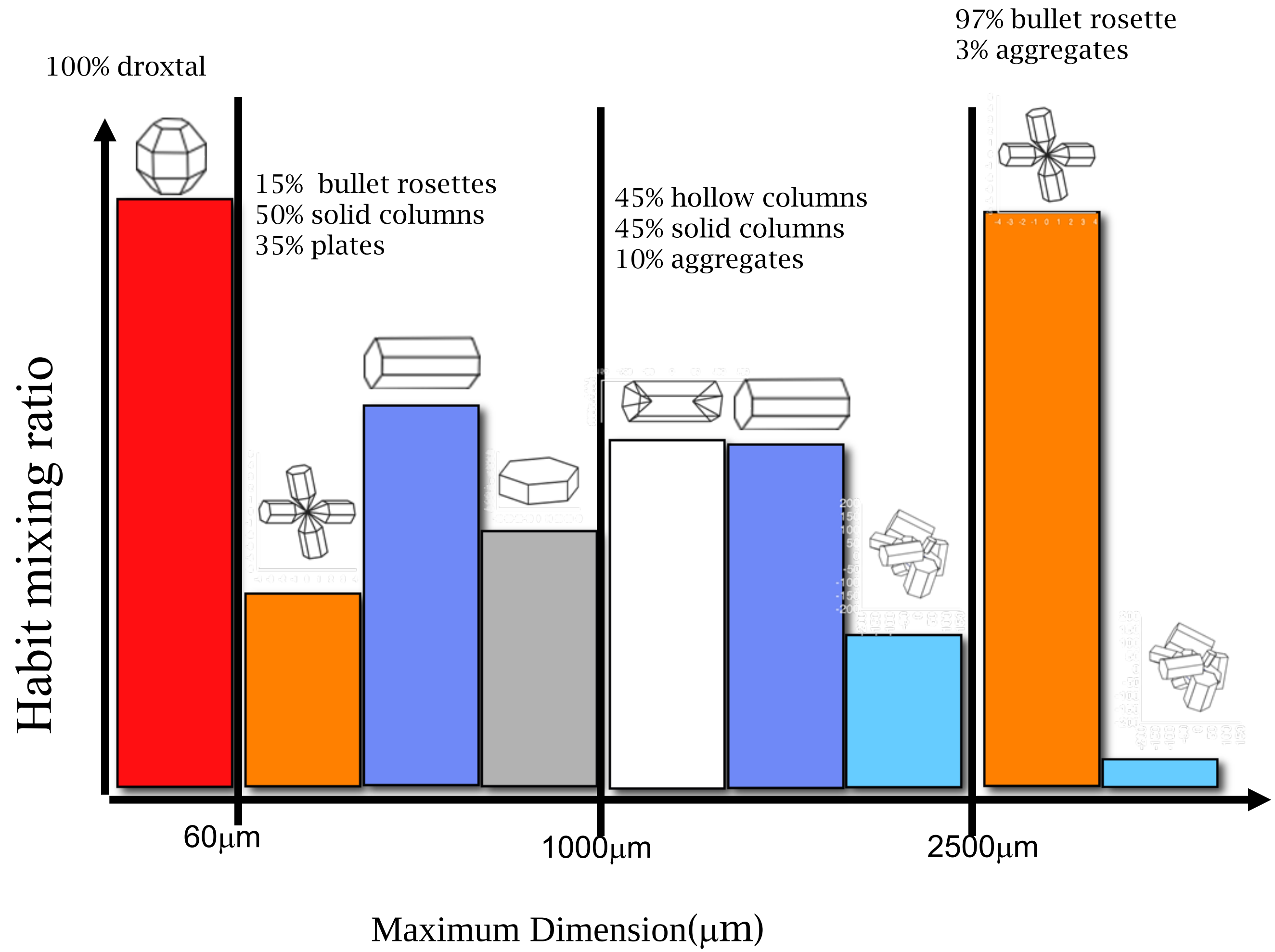

Cloud Scattering Properties-Phase Matrix Elements

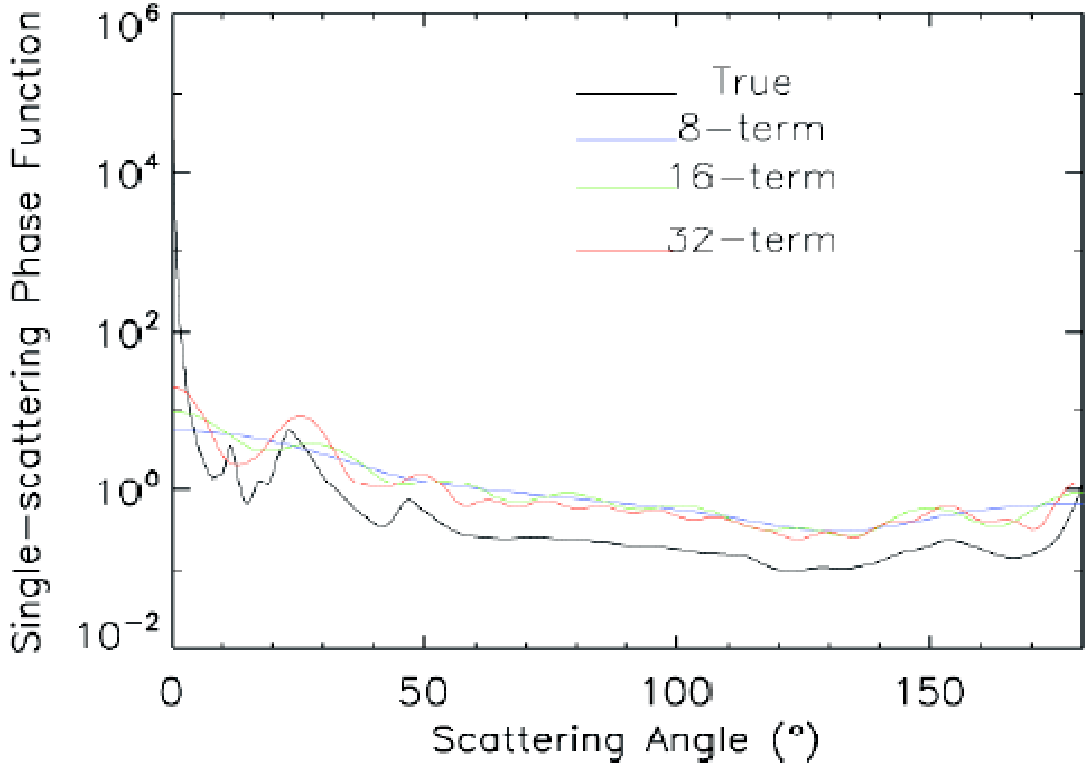

Fig. 2. Comparison of the single-scattering phase functions for ice crystals: original phase function (black), 8-term, 16-term, and 32-term Legendre polynomial expansions. The wavelength and effective particle size are λ=0.65 μm and De=60 μm, respectively.

Optical Parameters of Precipitation Sized Particles

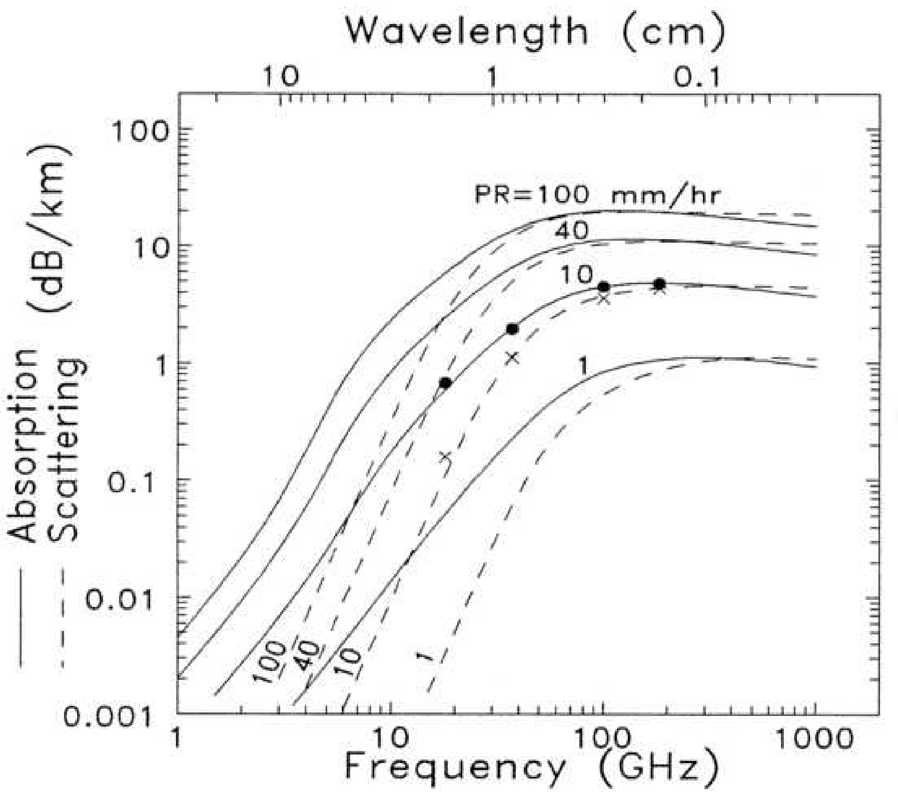

Rain

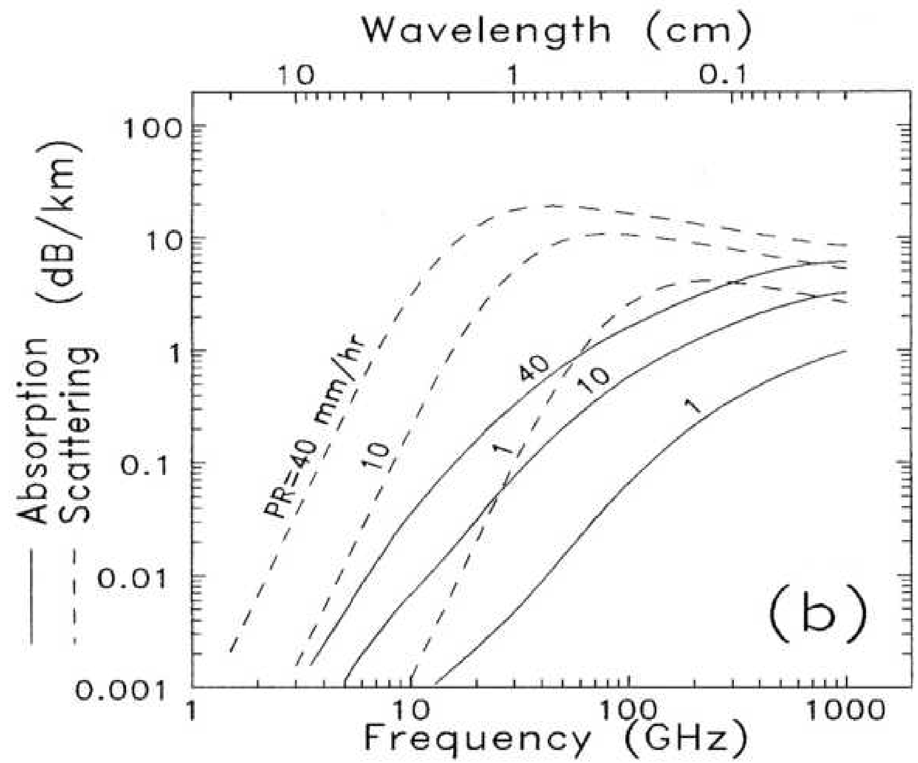

Graupel

Gasiewski, 199?

CRTM Aerosol Scattering Module

1. **Sulfur: DMS (Dimethyl sulfide), SO2, SO4, MSA (methanesulfonate)**
2. **Carbon: Hydrophobic BC/OC, hydrophilic BC/OC (water-like)**
3. **Dust: 8 bins: 0.1-0.18, 0.18-0.3, 0.3-0.6, 0.6-1, 1.0-1.8, 1.8-3.0, 3.0-6.0, 6.0-10.0 μm**
4. **Sea-salt: 4 bins: 0.1-0.5, 0.5-1.5, 1.5-5.0, 5.-10. μm**

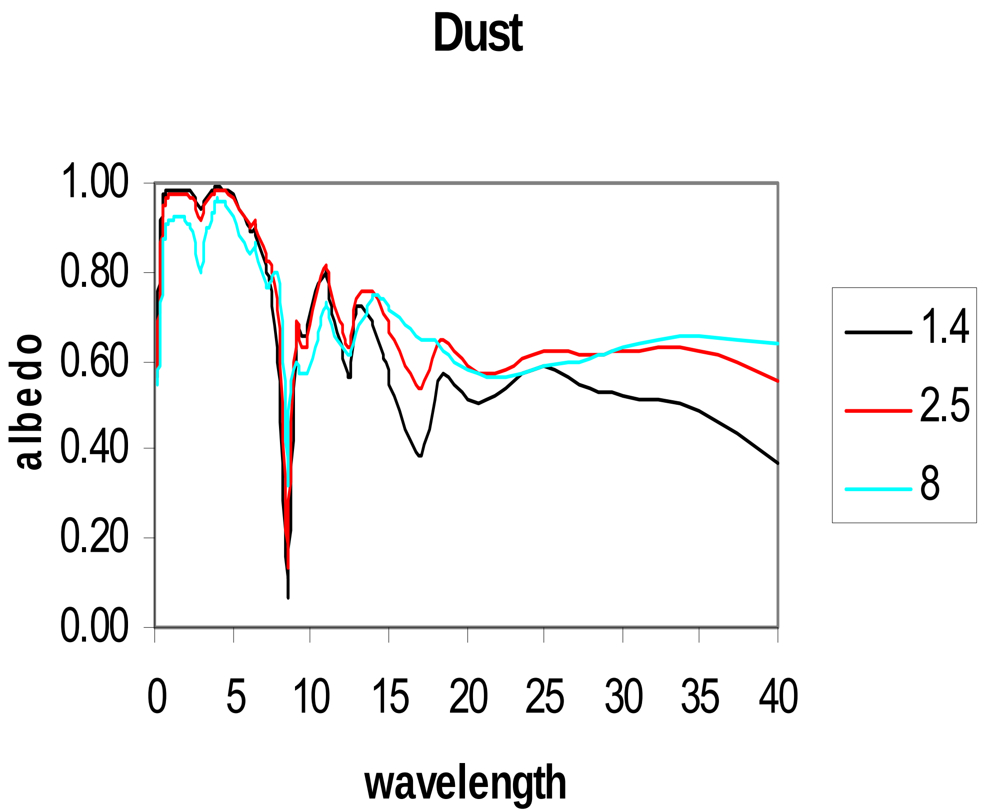

Aerosol Optical Model from GOCART

Global Model, Goddard Chemistry Aerosol Radiation and Transport (GOCART)

Species	Aerosol types in the CRTM
Dust	dust
Sea salt	sea salt ssam
	sea salt sscm
Organic carbon	dry organic carbon
	wet organic carbon
Black carbon	dry black carbon
	wet black carbon
Sulfate	sulfate

Lognormal size distribution, 35 size bins

Dust Aerosol Phase Matrix Elements

Sahara sand

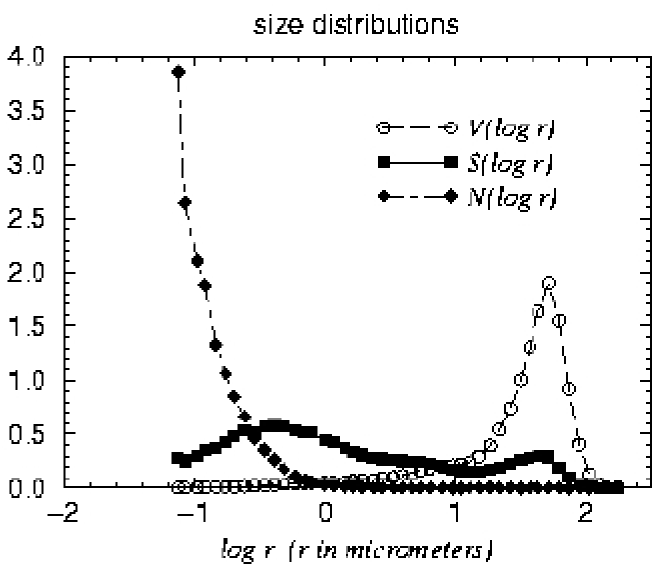

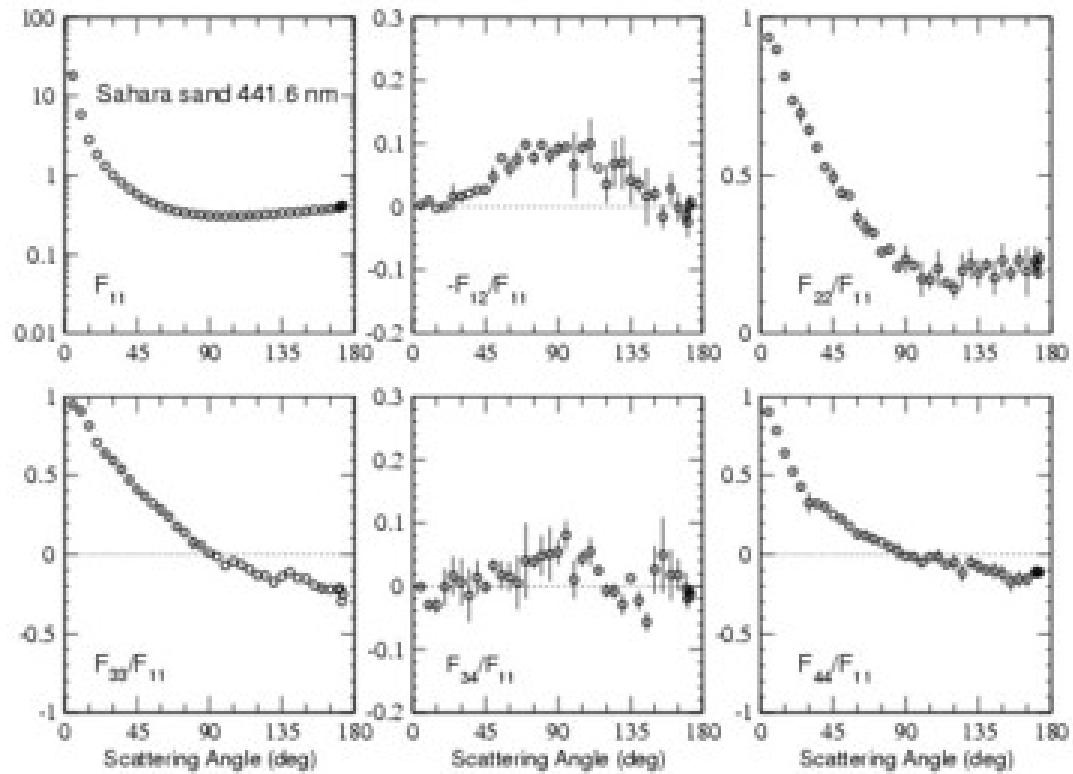

Phase functions

From Amsterdam Light Scattering Database

Aerosol Effect on NOAA-17 HIRS/3

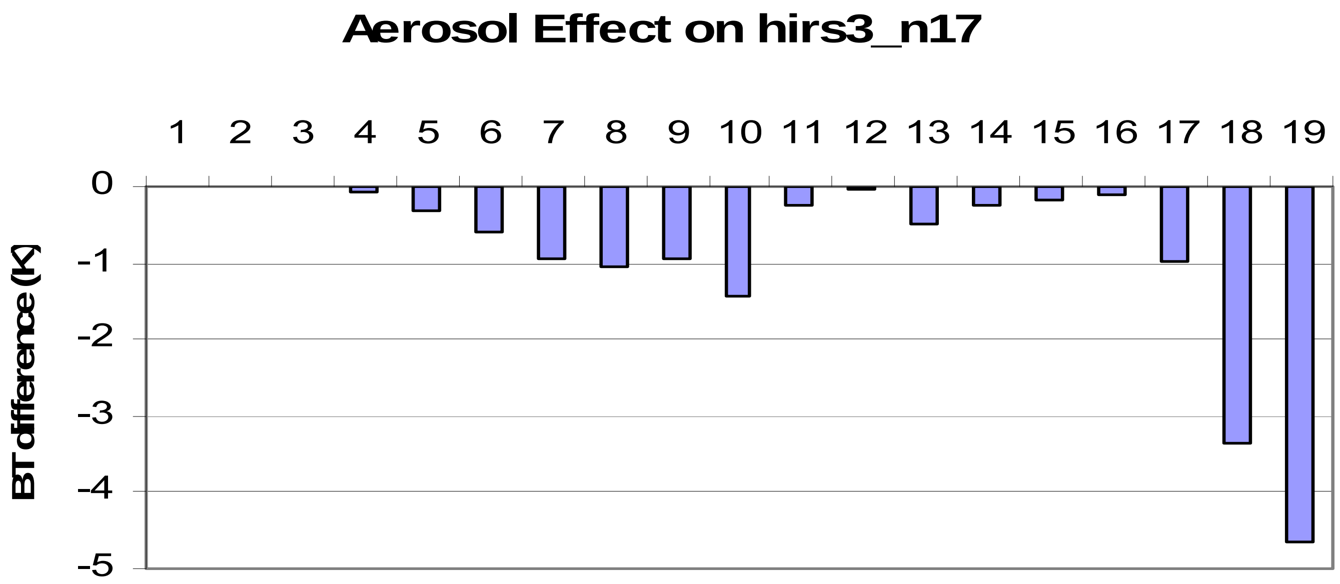

0.1 g/m^2 OC aerosol at layer 63 (300 hPa)

0.1 g/m^2 Dust aerosol at layer 80 (592 hPa)

0.1 g/m^2 Dust aerosol at layer 82 (639 hPa)

Infrared Surface Emissivity Data Base

- Water and snow has highest emissivity (> 0.9)
- Higher (lower) emissivity (reflectivity) at longer wavelength
- Desert displays largest variability and lower emissivity (especially at 4-5 micron, 8-10 micron
- Inconsistency among several data bases (JPL, NPOESS)

CRTM Baseline Model

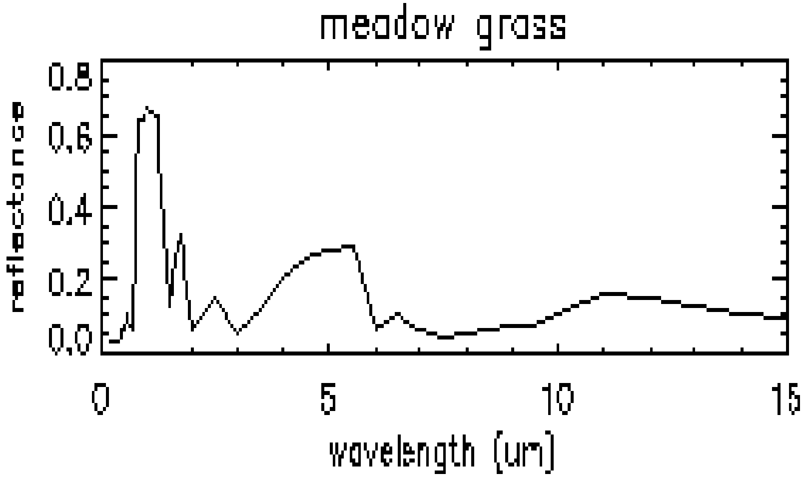

JPL Library

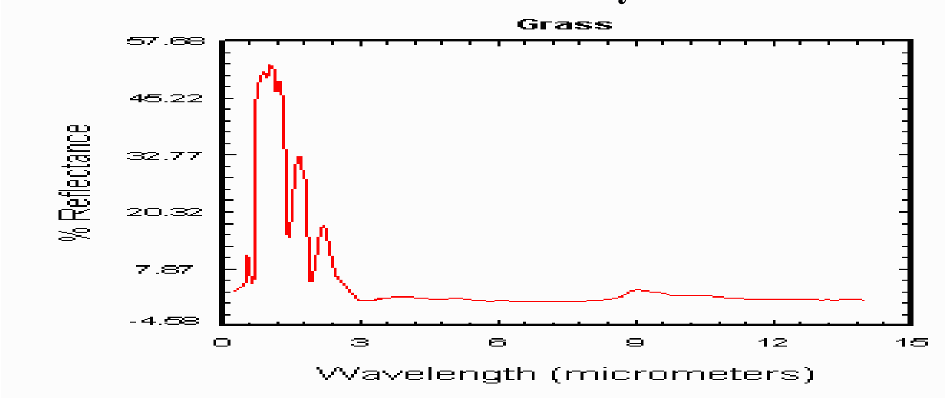

Intercomparison of CRTM with RTTOV/PFAAST

Jun Li/Tim Schmit

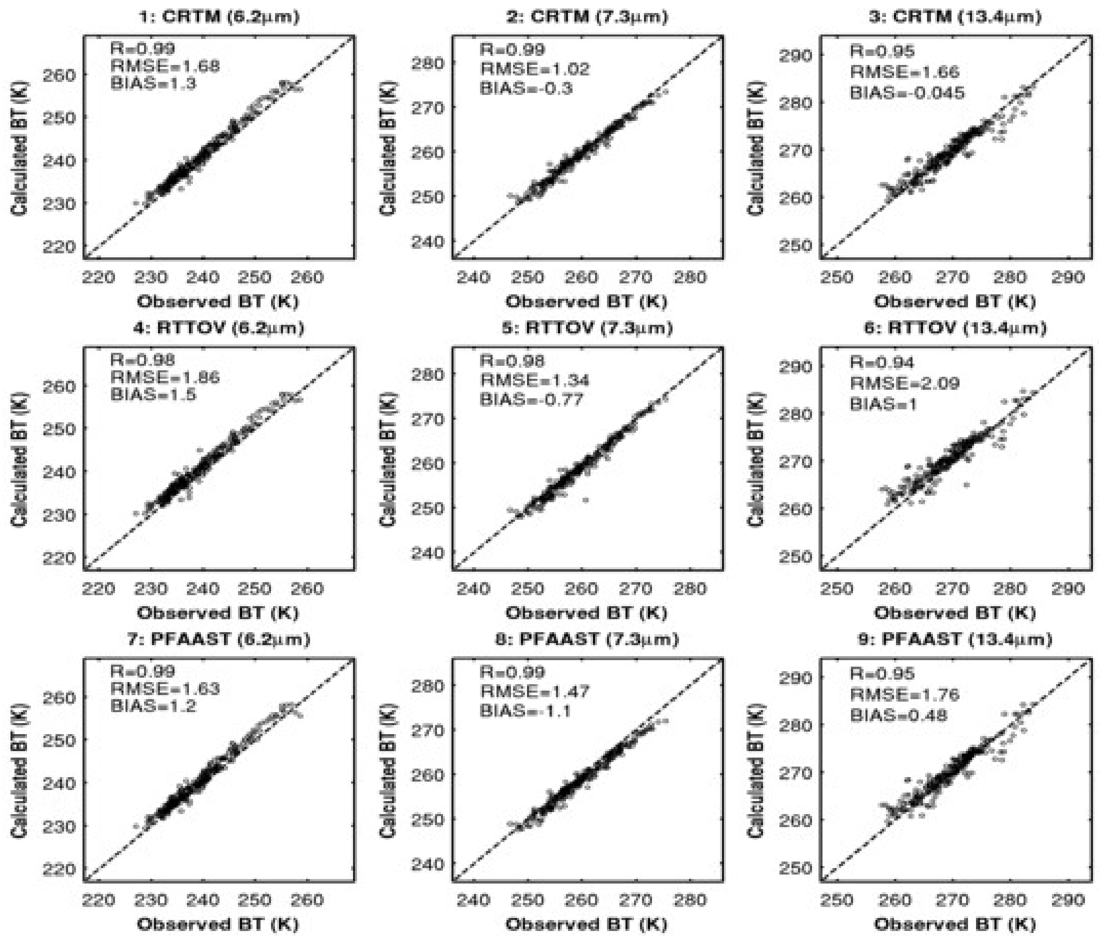

Simulated vs observed brightness temperatures using 457 radiosonde profiles

Weighting Functions at GOES-R ABI water vapor-absorbing bands

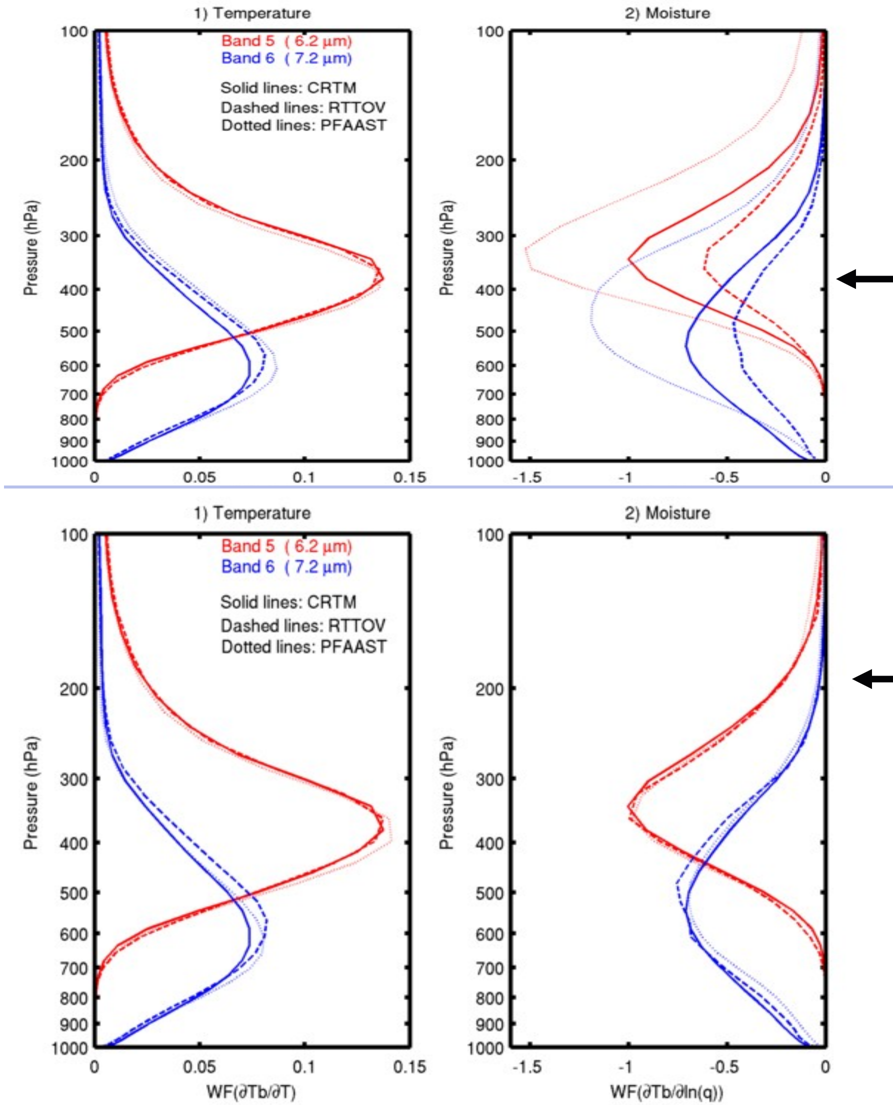

Internal Jacobian schemes

Perturbation method

Assumption: surface emissivity = 0.98, local zenith angle = 0 deg., and skin temperature = 300 K

Profile RMSE retrieved from ABI by CRTM and RTTOV

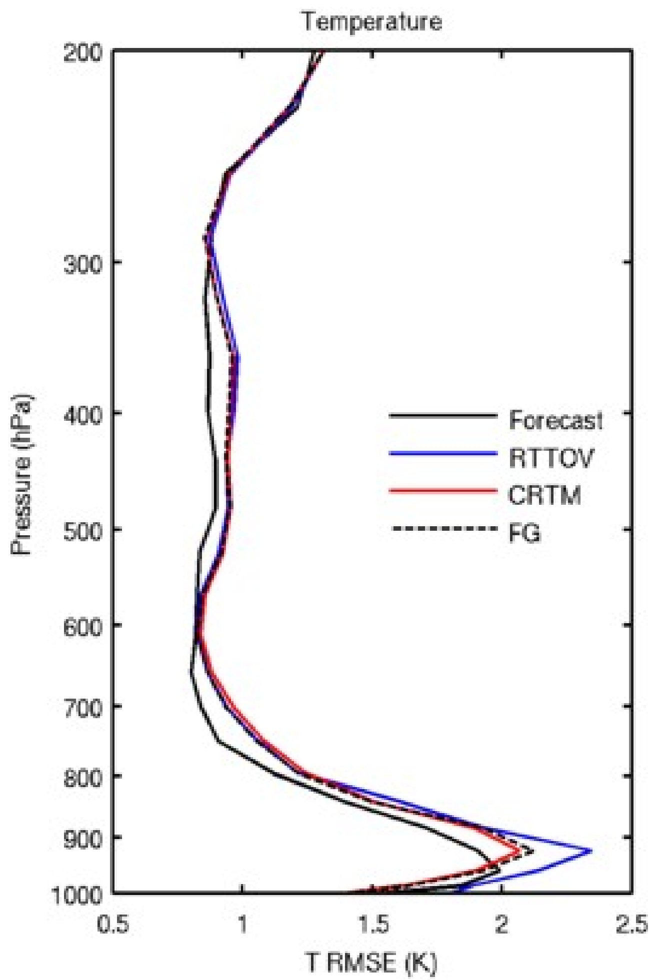

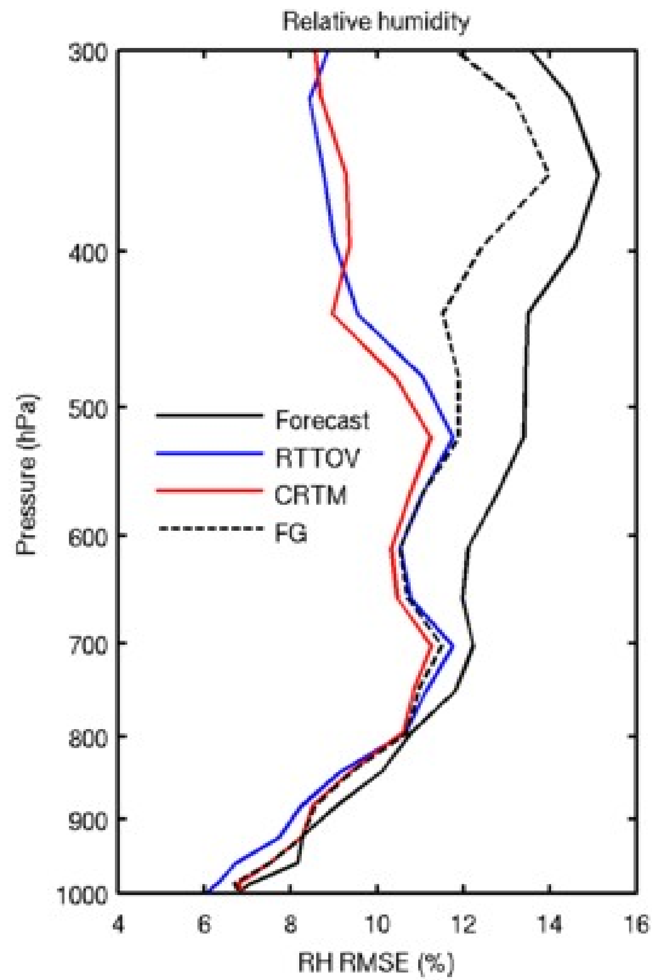

Profile RMSE retrieved from ABI by CRTM, RTTOV and PFAAST

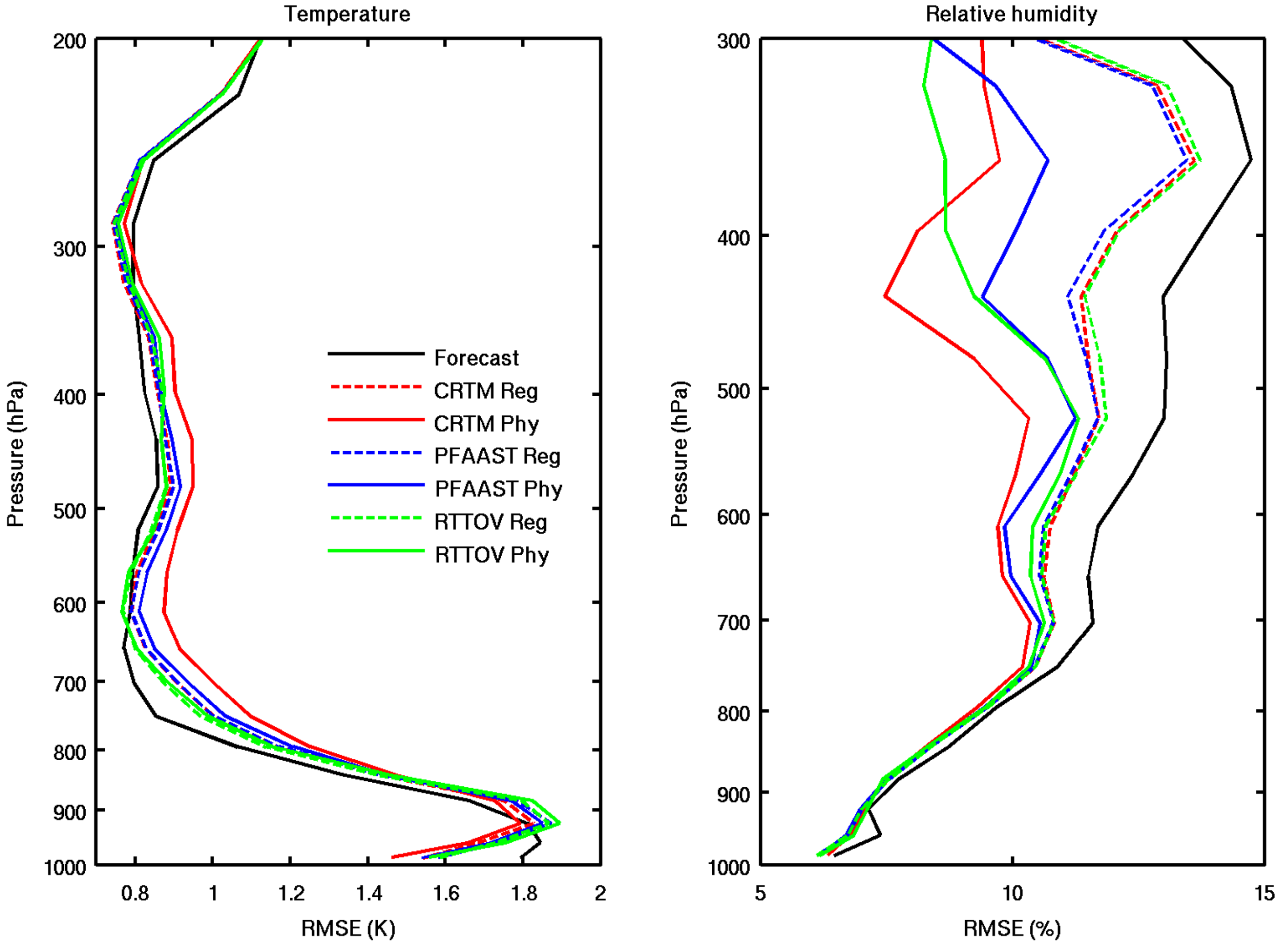

CRTM Surface Emissivity Module

Ocean

Sea Ice

Snow

Canopy (bare soil)

Desert

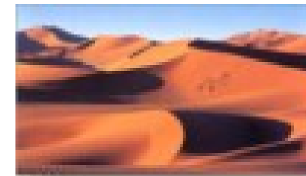

Microwave land emissivity model (Weng et al., 2001) and desert emissivity data base

NPOESS Infrared emissivity data base

Empirical snow and sea ice microwave emissivity data base (Yan and Weng, 2003; 2008)

New two layer snow emissivity model (Yan, 2008)

FASTEM microwave emissivity model from (English and Hewison, 1998)
IR emissivity model (Wu and Smith, 1991; van Delst et al., 2001)

Microwave Surface Emissivity

Open water – lower emissivity/higher polarization, increase with frequency (emission type)

Snow/desert/sea ice – high variability, higher polarization, decrease with frequency (scattering type)

Canopy – high emissivity and less frequency dependence

Bare soil (other than deserts) - High emissivity, depend on sand/clay/silt compositions

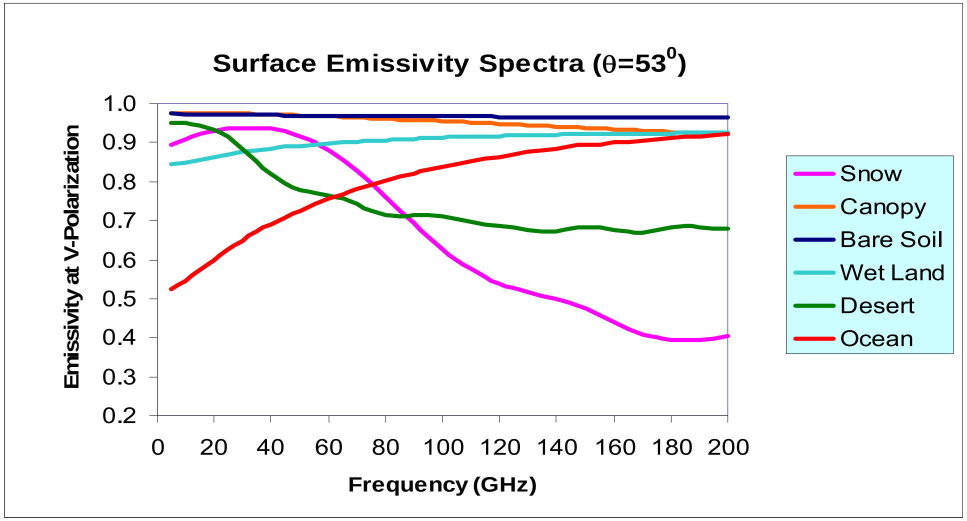

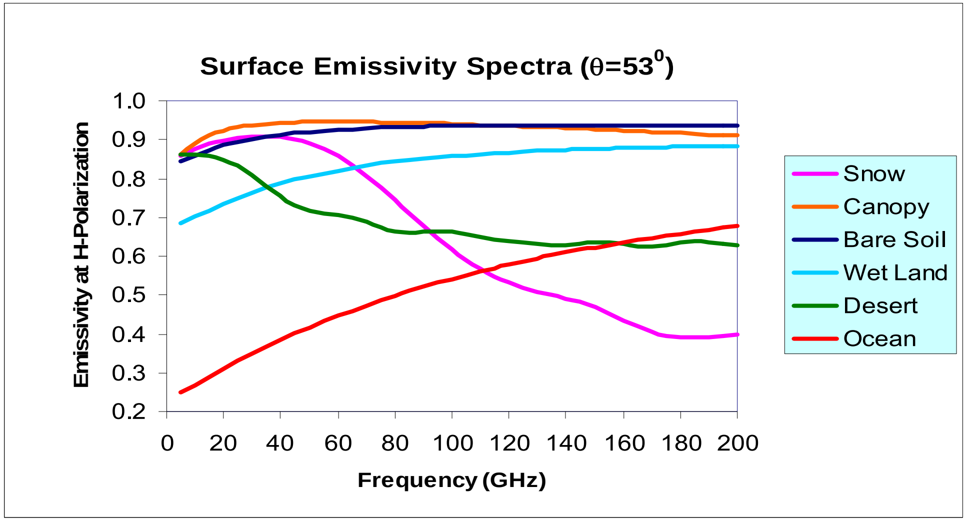

Summary

1. **Line by line calculations**:
   - Lorenz absorption, plus self and foreign broading
   - Doppler shift and zeeman effects
   - accurate but time consuming
2. **Fast gas absorption models**:
   - use a number of predictors to get polynomial fits to LBL
   - instrument response function
3. **Cloud and aerosol scattering**:
   - Spheres - Mie theory
   - Nonspherical-T-matrix; Discrete dipole approximation
   - LUT: scattering&absorption coefficients, phase matrix- polynomial expansion
4. **Forward radiative transfer schemes**
   - 2 streams
   - Discrete ordinate method
   - Double &adding
   - Successive order of iteration
5. **Surface emissivity variations**: Large and unpredictable over land